ERDC/CHL SR-16-1

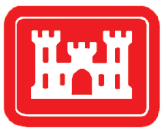

US Army Corps
of Engineers®
Engineer Research and
Development Center

ERDC
INNOVATIVE SOLUTIONS
for a safer, better world

Combined Wave and Current Bottom Boundary Layers: A Review

Richard Styles and Duncan Bryant

March 2016

Coastal and Hydraulics Laboratory

The U.S. Army Engineer Research and Development Center (ERDC) solves the nation's toughest engineering and environmental challenges. ERDC develops innovative solutions in civil and military engineering, geospatial sciences, water resources, and environmental sciences for the Army, the Department of Defense, civilian agencies, and our nation's public good. Find out more at www.erdc.usace.army.mil.

To search for other technical reports published by ERDC, visit the ERDC online library at http://acwc.sdp.sirsi.net/client/default.

ERDC/CHL SR-16-1
March 2016

Combined Wave and Current Bottom Boundary Layers: A Review

Richard Styles and Duncan Bryant

Coastal and Hydraulics Laboratory
U.S. Army Engineer Research and Development Center
3909 Halls Ferry Road
Vicksburg MS 39180-6199

Final report

Prepared for U.S. Army Corps of Engineers
Washington, DC 20314-1000

Under Section 219 Center for Directed Research

Abstract

This Coastal and Hydraulics Engineering Special Report (SR) presents a general review of research in combined wave and current bottom boundary layers including laboratory, field and model studies. The purpose of this SR is to chronicle the state-of-the-art in boundary layer research in order to identify research gaps and obtain guidance for developing and improving the next generation of combined wave and current bottom boundary layer models. One of the key research focus areas identified in this report is fine-grained sediment transport processes in combined wave and current flows. Critical research gaps exist in the following areas: (1) the role of oblique waves and currents on bottom stress and flow kinematics, (2) the effect of wave asymmetry in combined flows and how this drives mass transport, (3) the process of wave transition in shallow water in the presence of strong alongshore currents, (4) the interaction between oblique waves and currents over a sediment bottom, and (5) the validity and performance limitations of existing bottom boundary layer models under the above conditions. Progress towards understanding these research questions hinges on experimental programs to measure sediment, waves, morphology, and currents under a range of forcing conditions.

Contents

Figures and Tables

Figures

Tables

Preface

The work was performed by the Coastal Engineering Branch (HNC) and the Coastal Processes Branch (HFC) of the Navigation Division (HN), and Flood and Storm Protection Division (HF), respectively, U.S. Army Engineer Research and Development Center, Coastal and Hydraulics Laboratory (ERDC-CHL). At the time of publication, Tanya Beck was Chief, HNC; Dr. Mark Gravens was Chief, HFC; Dr. Jackie Pettway was Chief, HN; and Dr. Ty Wamsley was Chief, HF. The Deputy Director of ERDC-CHL was Dr. Kevin Berry, and the Director was José E. Sánchez.

COL Bryan S. Green was the Commander of ERDC, and Dr. Jeffery P. Holland was the Director.

1 Bottom Boundary Layer Models

1.1 Theoretical models

Modern theories of combined wave and current flows can be traced back to Lundgren (1972) who developed a simple one-dimensional (1D) model for the mean current in the presence of waves but did not include the nonlinear interaction between the wave and current stress components. The first study to include nonlinear effects was achieved, independently, by Smith (1977) and Grant (1977). The work of Grant (1977) was later reported in Grant and Madsen (1979). Both the Smith (1977) and Grant and Madsen (1979) models used simple, time-invariant, linear eddy viscosities and concentrated on flows very near the bed. The Smith (1977) model was developed for waves and currents flowing in the same direction while Grant and Madsen (1979) included waves and currents at arbitrary angles. Grant and Madsen (1979) theorized that the basic momentum transfer mechanisms in steady flow could be applied to the time-averaged wave and current flow. In the near bed region, momentum transfer is driven by shear stresses, which are routinely expressed in terms of an eddy diffusivity leading Grant and Madsen (1979) to adopt the following simple, two-layer eddy viscosity (K) to close the fluid momentum equation:

$$\begin{aligned} K &= \kappa u_{*cw} z \qquad z < \delta_{cw} \\ K &= \kappa u_{*c} z \qquad z > \delta_{cw} \end{aligned} \tag{1}$$

where κ is von Karman's constant (0.4), z is the vertical coordinate, u_{*cw} is the shear velocity associated with the combined flow, u_{*c} is the shear velocity for the current, and δ_{cw} is the wave boundary layer height. Within the wave boundary layer, the combined wave and current shear stress contributes to the shear-generated turbulence and associated momentum flux through u_{*cw}. Outside the wave boundary layer ($z > \delta_{cw}$), only the current contributes to the shear-generated turbulence as the oscillatory wave inhibits boundary layer growth, so the wave dynamics can be treated using potential flow theory.

Other early investigators adopted similar approaches but with slightly varying assumptions regarding the coupling between the wave and current

stress components leading primarily to differences in the vertical structure of the velocity profile (Christoffersen and Jonsson 1985; Fredsøe 1984). However, the basic concept of a multilayer structure consisting of a thin wave boundary layer embedded within a larger current boundary layer remain. Without high-resolution velocity profile data, it was difficult to validate these early models. Nielsen (1992) provides a good review of combined wave/current bottom boundary layer models prior to 1990 including validation studies, and Grant and Madsen (1986) provide a review of boundary layer theory.

The Grant and Madsen (1979) eddy viscosity is discontinuous at the top of the wave boundary layer leading to an artificial kink in the solution for the velocity profile. In addition, a linearly increasing eddy viscosity does not accurately represent the momentum flux in the outer wave boundary layer, since it is known that shear-induced turbulence production is reduced (Jensen et al. 1989; Jonsson and Carlsen 1976; Sleath 1987). In order to maintain a continuous eddy viscosity that also represents shear production in the outer wave boundary layer, Wikramanayake and Madsen (1991) and Styles and Glenn (2000) adopted the following three-layer form:

$$\begin{aligned} K &= \kappa u_{*cw} z \qquad z < z_1 \\ K &= \kappa u_{*cw} z_1 \qquad z_1 < z < z_2 \\ K &= \kappa u_{*c} z \qquad z > z_2 \end{aligned} \tag{2}$$

where z_1 is an arbitrary length scale that is some fraction of the wave boundary layer height and $z_2 = z_1 u_{*cw}/u_{*c}$, which is determined by matching the eddy viscosities at $z = z_2$. The added constant layer between z_1 and z_2 preserves continuity in the profile and more accurately represents the shear production in the outer wave boundary layer. It also leads to smooth profiles for the velocity and maintains u_{*cw} and u_{*c} as the characteristic velocity scales within and outside the wave boundary layer, respectively.

Owing to the growing number of 1D bottom boundary layer models, Soulsby et al. (1993) conducted an intercomparison between several widely reported existing combined flow models and data (see Soulsby et al. [1993] for a list of models). They noted that running the wave/current boundary layer models was computationally expensive and developed a

single parametric formula that calculates the solutions of the existing models for a wide range of wave and current conditions. Using their notation, the functions to compute the stress components are

$$y = x\left[1 + bx^{p}\left(1 - x\right)^{q}\right]$$
$$Y = 1 + ax^{m}\left(1 - x\right)^{n} \tag{3}$$

where a, m, n, b, p, and q are fitting parameters unique to each model. The variables are defined as

$$Y = \frac{\tau_{mx}}{\left(\tau_c + \tau_w\right)} \quad y = \frac{\tau_m}{\left(\tau_c + \tau_w\right)} \quad x = \frac{\tau_c}{\left(\tau_c + \tau_w\right)} \tag{4}$$

where τ_m is the combined bottom shear stress for the wave and current, τ_c is the time-averaged shear stress for the current, τ_w is the maximum shear stress for the wave, and τ_{mx} is the combined maximum shear stress. This approach produces a simplified method to compute the shear stresses and associated velocity profiles for combined flows in a computationally efficient manner by using a single stable polynomial and a small set of constants that can be maintained in a library file.

There have been a wide variety of other combined flow models developed and tested since this early work. Malarkey and Davies (1998) modified the Grant and Madsen (1979) analytical model to include first and second harmonic time variations in the eddy viscosity. Including time variation reduces the nonlinear dependence on the current stress especially when the current dominates the waves and produces a veering in the current vector within the wave boundary layer. Other investigators have developed analytical models based on an eddy viscosity closure but are not discussed explicitly as they generally fall within the overall framework presented here (Nielsen 1992; Shi and Wang 2008; You 1996).

1.2 Numerical models

In addition to the analytical models discussed above, numerical models that include turbulence kinetic energy closure, thus permitting more complex eddy viscosity profiles, have been developed. Davies et al. (1988)

developed a 1D numerical model that expressed the eddy viscosity in terms of a dynamic mixing length (l) and turbulence kinetic energy (q):

$$K \sim \sqrt{q} l \tag{5}$$

These early results were similar to previous analytical treatments, but they also focused on the effect of waves and currents at arbitrary angles. Maximum instantaneous shear stress decreased as the angle between the wave and current (φ_{cw}) increased owing to the decoupling of the nonlinear wave and current stress components. This increased the magnitude of the current as the reduction in bottom stress decreased the upward flux of low momentum fluid away from the wave boundary layer. The asymmetry in mass flux during the wave cycle, in which the wave vector forms an acute angle to the current during the first half of the wave cycle and an obtuse angle during the second half, produced a rotation in the current profile.

With the advent of modern computational platforms, numerical modeling of the 1D wave and current boundary layer has become more efficient leading to a growth in the number of reported studies (see Shi and Wang, [2008] for a review). Numerical models generally fall into two categories based upon the turbulence closure method (Shi and Wang 2008). One-equation models express the eddy viscosity in terms of q and a mixing length similar to Equation (5). A prognostic equation for the turbulence kinetic energy is solved numerically, and the mixing length is either prescribed or likewise written in terms of other variables and solved numerically. Two-equation models express the eddy viscosity in terms of q and turbulence kinetic energy dissipation (ε):

$$K \sim \frac{q^2}{\varepsilon} \tag{6}$$

Prognostic equations are solved iteratively for q, ε, and the momentum equations requiring greater computational resources as the number of floating point operations and variables increases. The high-resolution output permits direct comparisons with data and provides insight into relative contribution of the various terms to the momentum balance. Numerical models are also used to explore arbitrary wave and current intensities including the limiting case of pure waves or pure currents.

Shi and Wang (2008) used a two-equation model (q, ε) to investigate combined flows and demonstrated good agreement with the laboratory profile data of Van Doorn (1981) especially within the wave boundary layer. The model accurately predicted the reduction in mean current shear observed in the wave boundary layer as well as the wave velocity overshoot at the top of the wave boundary layer. Li and O'Connor (2007) modified the commercial code FLUENT to model the fine scale vertical and horizontal structure of wave, current, and sediment concentration profiles above a rippled bed. They noted that in the combined flow case, vortices tended to remain low in the trough and that eddy shedding over the ripples occurred earlier in the wave cycle. The addition of the mean current when added to the accelerating wave increased the kinetic energy leading to earlier eddy ejection. Comparison between laboratory data and the model showed good agreement in the structure of the flow and concentration above the ripples. Faraci et al. (2008) also used a two-equation numerical model to study flow over ripples for arbitrary φ_{cw}. Comparisons to laboratory measurements in which the wave was at right angles to the current for both flat and rippled beds showed a decrease in bottom shear stress for the flat-bed case and a reduction in current velocity near the bottom for the rippled case. They were only able to examine cases in which the waves were stronger than the currents owing to the experimental setup so that results to examine the limit of pure currents at arbitrary angles to the waves were not provided.

1.3 Sediment transport models

Sediment transport models similarly have evolved in conjunction with wave and current boundary layer models owing to the practical need to understand sediment transport and associated geomorphological processes. Unlike the nonlinear boundary layer theories posed by Smith (1977) and Grant and Madsen (1979) in the 1970s, modern theories on sediment resuspension can be traced back to Rouse (1937). Rouse (1937) theorized that the upward turbulent flux of sediment balances the tendency for particle settling under the action of gravity, thus greatly simplifying the governing equations and laying the foundation for modern theoretical studies of sediment transport. Lumley (1978) established quantitative guidelines to identify conditions for which the Rouse (1937) theory could be applied. Smith (1977) also included in his combined wave and current model algorithms to compute suspended sediment concentration profiles using the original theories introduced by Rouse (1937). Wiberg and Smith (1983) included a correction for suspended sediment-induced stratification

to the Smith (1977) model, while Glenn and Grant (1987) did the same for the Grant and Madsen (1979) model. Wikramanayake and Madsen (1992) derived a suspended sediment concentration model under neutral conditions for use with the Madsen and Wikramanayake (1991) wave and current model. Styles and Glenn (2000) extended the work of Glenn and Grant (1987) and included a correction for suspended sediment induced stratification for the three-layer eddy viscosity model (Equation 2). These analytical models provide solutions to the concentration profile for arbitrary sediment characteristics and multiple grain size classes.

The majority of the numerical models discussed above also included sediment transport formulations for combined flows. For the linear models, the stronger waves resuspend sediment while the current acts to transport the suspended material. Wave asymmetries, bedforms, and stratification add complexity to this simple conceptual model, but the basic assumption that the much stronger waves resuspend sediment in an otherwise pure current regime has been documented in many studies. For a review of sediment transport studies see Van Rijn (2007a), Van Rijn (2007b), and applications of numerical models, see Papanicolaou et al. (2008).

1.4 Example model predictions

Vertical profiles of current, sediment concentration, and sediment flux are depicted in Figures 1 and 2. The results were computed using the Styles and Glenn (2000) bottom boundary layer model and represent typical wave and current conditions (Figure 1) and the limiting case of strong waves in the presence of weak currents (Figure 2). The input parameters include the near bottom wave orbital velocity amplitude (u_b), the near-bed wave excursion amplitude (A_b), and the time-averaged current at a known height above the bottom (u_r). Given wave height, wave period, and water depth, the wave parameters can be computed using linear wave theory (Dean and Dalrymple 1991). The current must be measured at a known height above the bottom within the constant stress layer.

Within the wave boundary layer, the current profile shows less variation with height due to the upward flux of low-momentum fluid away from the bed. The greater momentum flux is due to stronger turbulence in the wave boundary layer, which reduces vertical shear. The profile shape transitions to a linear increase with height in the outer wave boundary layer, where the stress due to the wave vanishes. Outside the wave boundary layer, the profile is analogous to a typical log-layer without waves. Sediment

concentrations are highest at the bed and decrease with height as the stresses are reduced. Like the current, there is a transition in the outer wave boundary layer above which the concentration rapidly decays. The presence of the waves reduces the vertical gradient so that concentrations are higher within the wave boundary layer than for a pure current. The sediment transport is defined as the product of the concentration and current at a given height. Transport profiles initially increase as a function of height as the increase in current speed dominates over the reduction in concentration. Higher in the water column, transport asymptotically decreases as the concentrations become infinitesimally small. The results are likewise sensitive to grain size with the smaller sizes showing higher concentrations and greater transport. Given their lower mass, the smaller grains are lifted higher off the bed, increasing the water column's capacity to support a greater number of particles.

Model sensitivity to the relative strength of the wave and current is illustrated in the case of strong waves in the presence of weak currents (Figure 2). While the qualitative profile shapes are similar, concentration rapidly attenuates outside the wave boundary layer due to the weaker current stress. Transport is reduced and confined primarily to the lower 1 m of the water column.

Figure 1. Vertical profiles of the current, suspended sediment concentration, and sediment transport. Concentration is in units of microliters per liter (µL/L). The legend denotes grain size class in µm (microns). The input wave and current conditions are bottom excursion amplitude (A_b = 50 cm), bottom orbital velocity (u_b = 40 cm/s), and mean current (u_r = 60 cm/s) at a height of 100 cm.

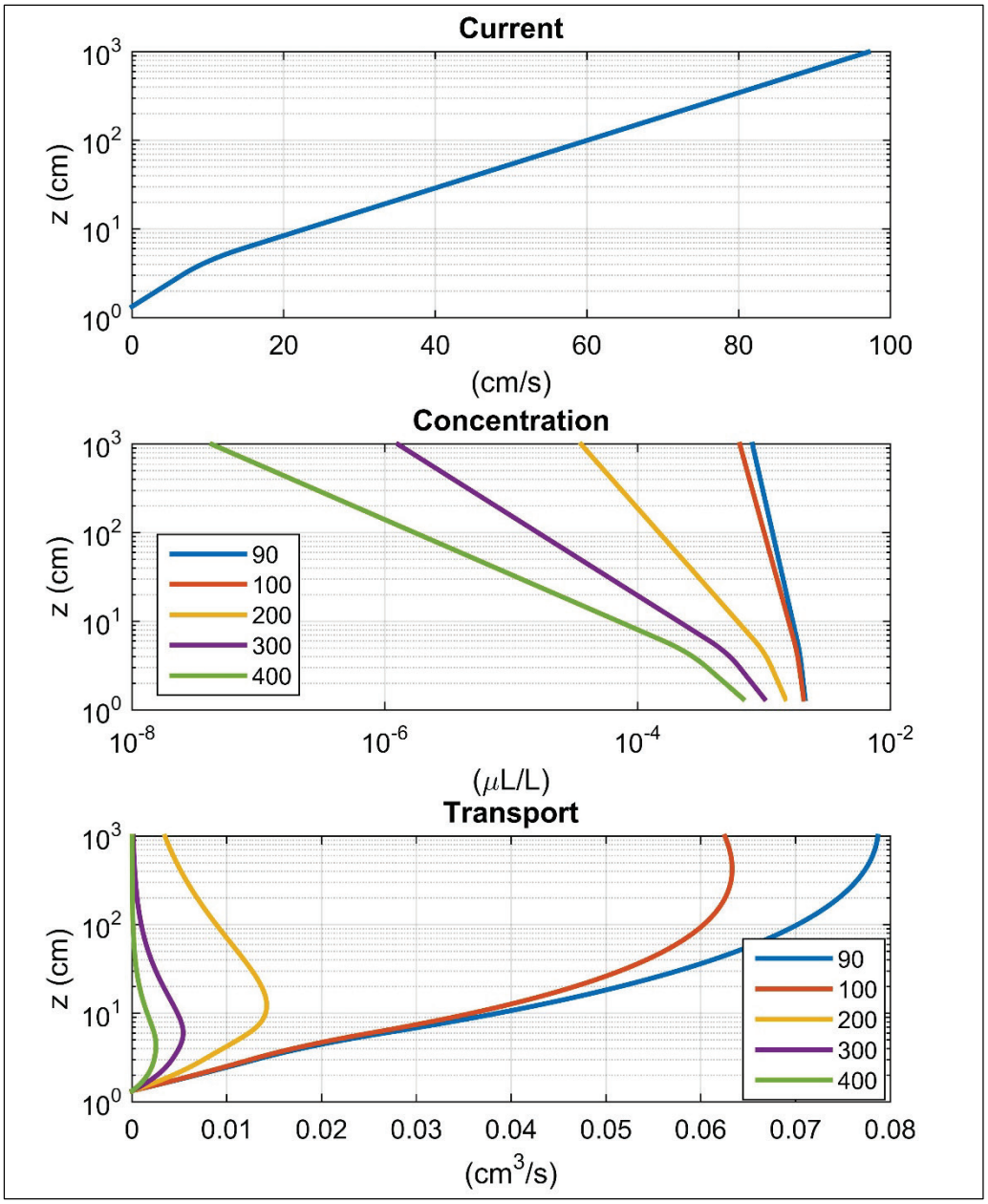

Figure 2. Vertical profiles of the current, suspended sediment concentration, and sediment transport. The legend denotes grain size class in μm. The input wave and current conditions are bottom excursion amplitude (A_b = 140 cm), bottom orbital velocity (u_b = 100 cm/s), and mean current (u_r = 5 cm/s) at a height of 100 cm.

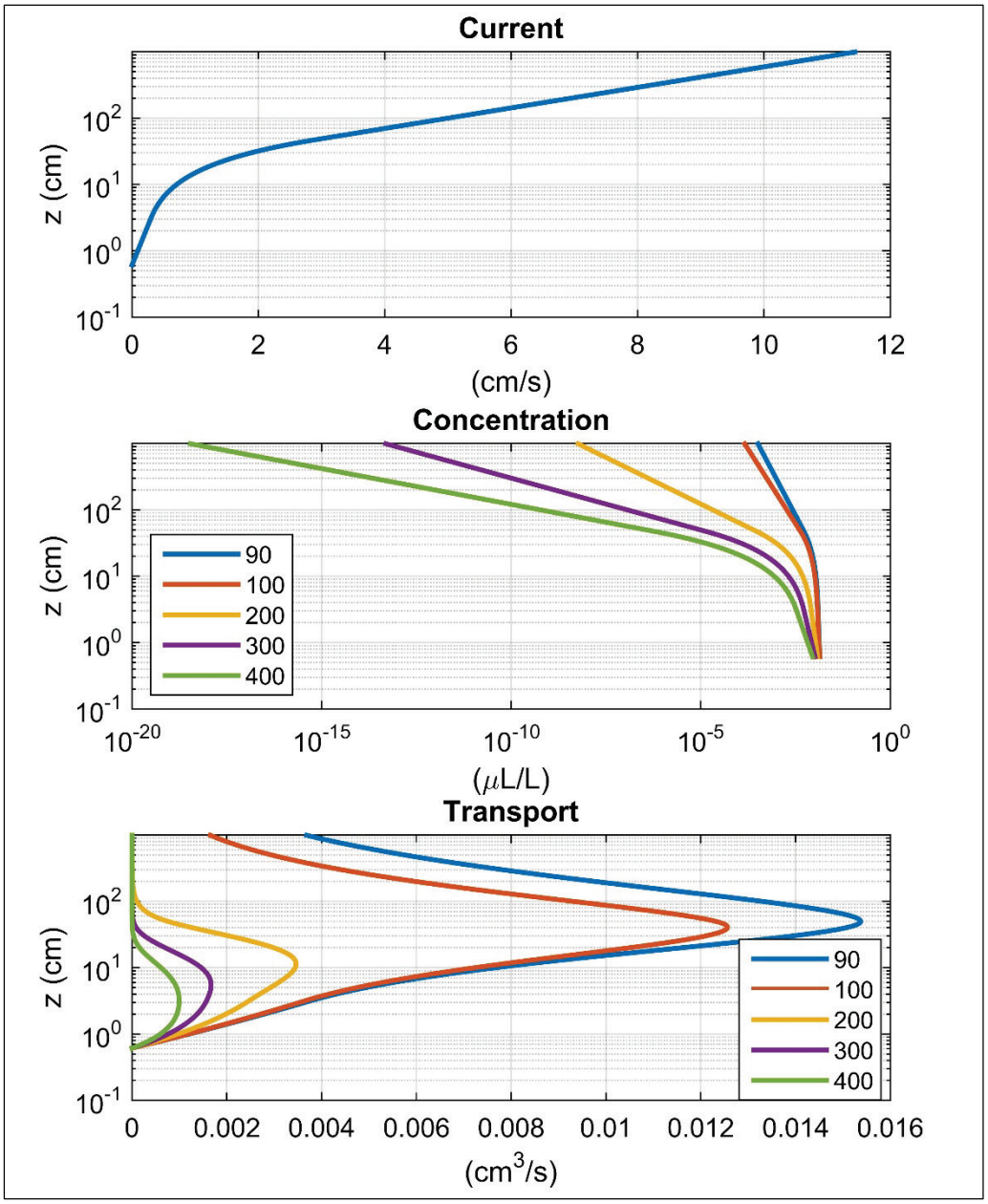

2 Major Field Programs of Boundary Layer Processes

2.1 CODE and STRESS – Northern California

In conjunction with modeling studies of flow and sediment transport for combined waves and currents, a number of related observational programs have been conducted over the past several decades. One of the earliest large-scale field studies was conducted as part of the Coastal Ocean Dynamics Experiment (CODE) during the spring and summer of 1981 (Allen et al. 1982). During early June of that year, instrumented bottom boundary layer tripods equipped with state-of-the-art current sensors were deployed at depths of 30 and 90 m off the northern California coast. Results from the 90 m deployment reported by Grant et al. (1984) demonstrated the importance of wave/current interaction in determining bottom stress and confirmed the presence of logarithmic velocity profiles in the continental shelf bottom boundary layer. Grant et al. (1984) also showed that bottom stress estimates using the Grant and Madsen (1979) model were typically within 10%–15% of those measured. Also on the northern California shelf, but during a winter storm in December 1979, Cacchione et al. (1987) measured logarithmic velocity profiles near the bed in 85 m of water and suggested that high shear stress events due to combined wave and current flow could be a major factor in controlling the distribution of surficial sediment. Estimates of shear velocity obtained from a bottom boundary layer tripod were similarly shown to be in good agreement with the Grant and Madsen (1979) model.

A decade after CODE, researchers returned to the northern California shelf as part of the Sediment TRansport on Shelves and Slopes (STRESS) experiment (Lynch et al. 1997; Sherwood et al. 1994; Wiberg et al. 1994). Occupying some of the original mooring sites used during CODE, researchers engaged in a comprehensive investigation of sediment resuspension and flux using state-of-the-art current, optical, and acoustical backscatter sensors. These instruments measured current and suspended sediment concentration profiles, particle size spectra, particle settling velocity, and microtopography (Sherwood et al. 1994). Unlike CODE, which was conducted during the spring and summer upwelling season, the initial phase of STRESS focused on the storm season during the winter months of

1990–1991. Sediment resuspension information obtained during storms in 90 m water depth confirmed the importance of wave/current interaction on the vertical distribution of suspended sediment (Lynch et al. 1997) and revealed a distinct transition layer in the measured profiles similar to that predicted in the Wikramanayake and Madsen (1992) suspended sediment concentration model. Additionally, instruments were used to determine suspended sediment particle size distribution and showed good agreement with grab samples and laser diffraction instruments designed to measure particle size spectra (Lynch et al. 1994).

2.2 U.S. East Coast

While CODE and STRESS experiments increased present theoretical and experimental knowledge on flow and sediment transport in boundary layers, both were conducted in relatively deep water with bottom sediment comprised mostly of silt. One of the earlier studies for a wide shallow shelf was conducted off the New Jersey coast by McClennen (1973). McClennen (1973) deployed individual current meters offshore of New Jersey in water depths ranging from 20 to 140 m and obtained velocity data to calculate sediment transport in combined wave and current flows. Using wave data from National Oceanic and Atmospheric Administration (NOAA) buoys in conjunction with his measured currents, McClennen (1973) calculated empirical relationships to describe the sand movement threshold. He further alluded to the now well-understood process of sediment transport in combined wave and current flows, where the waves act to suspend sediment while the mean current transports it horizontally. Wright et al. (1991) deployed boundary layer tripods in the Middle Atlantic Bight over a 3-year period in a depth of 7–17 m at two locations offshore of North Carolina to study cross-shore transport for a variety of conditions ranging from fair weather to storms. Currents were measured at four heights off the bed using two-component electromagnetic current meters (ECMs) at a sampling rate of 1 Hz, and suspended sediment was measured at five heights off the bed using optical backscatter sensors (OBS), which also sampled at 1 Hz. Madsen et al. (1993) deployed boundary layer tripods offshore of North Carolina in a water depth of 13 m using the same instrument package as Wright et al. (1991). Although the OBS sensors provide vertical profiles at five discrete heights, acoustic instruments, like the 5 MHz acoustical backscatter (ABS) deployed during STRESS, provide individual concentration estimates in 1 cm bins ranging from the sea bed up to approximately 50 cm. Lee and Hanes (1996) deployed a horizontal cross-bar attached to two vertical posts jetted into the sand in 3–4 m of water off the Atlantic

coast of Florida using optical and ABS sediment profiling instruments but only one ECM. Sediment concentration was adequately resolved, but the shear stress was calculated using the Madsen and Wikramanayake (1991) bottom boundary layer model. During high wave conditions, measured concentrations from the acoustic profiler showed fair agreement with the Wikramanayake and Madsen (1992) suspended sediment transport model. Trowbridge and Agrawal (1995) deployed a bottom boundary layer tripod off Duck, NC, in a water depth of approximately 6 m and obtained current profile measurements from 5 to 16 cm above the bed but did not investigate sediment resuspension.

None of the above shallow water studies on sandy shelves possessed the variety of instrumentation or the comprehensive scope of either CODE or STRESS. In the summers of 1994, 1995, and 1996, instrumented tripods equipped with wave and current sensors, OBS, ABS, altimeters, sector scanning sonars, and video cameras were deployed on the inner New Jersey shelf at the Long-Term Ecosystem Observatory in 15 m of water (LEO-15) site (Schofield et al. 2002; von Alt and Grassle 1992). The primary goals of this study were to use state-of-the art acoustical and optical sensors to measure current and suspended sediment concentration profiles, particle size spectra, particle settling velocity, and microtopography of the sea floor to produce a comprehensive dataset on flow and sediment transport for this shallow water environment. The availability of these high-resolution measurements, combined with updated theories on the physics of flow and sediment transport, provided the means for upgrading existing boundary layer models and gauging model performance using data obtained exclusively in a natural shallow water environment consisting primarily of medium-sized sand. Results from these studies led to validation of the Styles and Glenn (2000) combined wave current model and provided field measurements to improve ripple geometry models (Styles and Glenn 2002; Traykovski et al. 1999).

2.3 Adriatic Sea

In 2002 and 2003, a large international field program was conducted in the northern Adriatic Sea to examine sediment transport pathways and geological strata formation (Fox et al. 2004). Termed EuroSTRATAFORM, the study comprised an extensive observational component including bottom tripods, ship surveys, water column profiles, surface drifters, and bottom core samples. The United States Geological Survey (USGS) deployed two benthic tripods in 10 and 20 m water depths, respectively, equipped

with wave, current, turbidity, altimetry, and multibeam sonar sensors during winter and summer to capture seasonal variability in the primary forcing mechanisms. The observational program provided insight into the mechanisms of sediment transport in a shallow, semi-enclosed coastal setting with significant fine sediment supply from the Po River in northern Italy (Traykovski 2007). The program also included numerical modeling to investigate the role of episodic events and river discharge on sediment transport pathways and strata formation (Bever et al. 2009). Similar to the northern California shelf, gravity-driven flows were observed to be a dominant sediment transport mechanism for fined-grain material, and waves were the primary mechanism for initiating sediment motion.

2.4 Western Louisiana shelf

The U.S. Office of Naval Research (ONR) sponsored a field program aimed at characterizing energy loss and resulting decrease in wave height of waves propagating over a broad muddy shelf. The program was carried out between 2007 and 2010 on the western Louisiana shelf offshore of the Atchafalaya River. This region is characterized as wave dominated with a substantial supply of fined-grained sediments during high-discharge events. The program was designed to use cross-shelf arrays to measure wave attenuation and bottom sensors to measure sediment concentrations and seabed processes. The wave energy balance was closed by balancing wave attenuation, less wind inputs and white capping, with frictional losses at the seabed. Various investigators visited the site during the duration of the program, but the most heavily instrumented period was through the winter and summer of 2008. Bottom instrument frames included acoustic Doppler current profiles (ADCPs) to measure water column currents including fine-scale profiles near the bed, vertical pencil-beam sonars that penetrated the mud bottom to measure layer thickness, and bottom pressure sensors to measure waves and pressure fluctuations. Ship surveys included imaging technology to map the mud layer and vertical profiles of currents and water-quality parameters. High-resolution current meters provided estimates of turbulence statistics including dissipation rates and turbulence intensity in the near-bed layer.

Safak et al. (2013) used a spectral wave model and data to investigate wave energy dissipation induced by fluid mud. Measurements were made on the western Louisiana shelf in shallow depths (3–4 m) in the presence of mud layers that sometimes exceeded 10 cm thickness. They noted that sediment-induced dissipation was greatest during periods with high concentrations of

suspended sediment (> 10 grams per liter). Reworking of the near-bed layer by waves maintained a fluidized, viscous layer but with a thickness much less than typically formed under strong waves. Engelstad et al. (2013) noted that in addition to wave dissipation of the full energy spectra, the presence of mud suppressed the development of short fetch-generated waves. Sahin et al. (2012) used ABS and current measurements to follow the evolution of fluid-mud formation during an energetic storm. They noted that the sediment first became dilated due to water entrainment, followed by erosion during the most intense portion of the storm, and then deposition and reconsolidation. Utilizing a 1D model, they predicted critical shear stress to vary between 0.3 and 0.5 Pa. Bed-density estimates inferred from vertical exchange of sediments varied in the range of 1,030 and 1,200 kg/m^3. Both the stress and density were within estimates previously obtained in laboratory studies.

The above review highlights the evolution of observation programs by focusing on a select number of highly organized, large-scale, multi-institutional field programs. This does not constitute the majority of all previous work, as there have been a number of field and laboratory studies of smaller scope reported in the literature. Research efforts to further gauge the accuracy of existing models, to refine estimates of empirical coefficients, and to add new model capabilities (i.e., roughness formulations, time varying bedforms, wave asymmetry) have been carried out in a wide variety of environmental settings (for an overview, see Amoudry and Souza [2011]). The above review and accompanying citations serve as a guide to point the reader to specific experiments, but the major contributions to modern understanding of boundary layer physics have been summarized here.

3 Process Studies of Boundary Layer Parameters

In addition to the major field programs described above, a number of related experiments have advanced present understanding of key wave and current boundary layer processes. Research continues to evolve in this area as new theories and instrumentation evolve.

3.1 Bottom roughness

Bottom roughness is a fundamental parameter of boundary layer research. It is proportional to the hydraulic roughness, which scales the vertical coordinate within the constant stress layer and is often used to define the location of boundary fluxes of momentum and suspended sediment concentration in models. On continental shelves, roughness length is a function of a number of bed attributes including sand grains, wave and current bedforms, and for strong flow conditions, highly concentrated, near-bed sediment transport layers.

Conceptually, the physical roughness (k_b) is a function of the bedform dimensions

$$k_b = f\left(h_b, w_b, l_b, S_b\right) \tag{7}$$

where h_b, w_b, l_b, and S_b are the characteristic height, width, length, and spacing, respectively, of the protrusions (Wooding et al. 1973). On wave-dominated sandy shelves, ripples are prevalent features, and the relationship between the geometrical properties of ripples, such as ripple height, and the roughness has been an active area of research for many years (Gross et al. 1992; Inman 1957; Li and Amos 1998; Mathisen and Madsen 1996; Nielsen 1992; Styles and Glenn 2002; Tolman 1994; Traykovski et al. 1999; Wiberg and Harris 1994).

3.1.1 Wave-generated ripple roughness

On the basis of the ripple data of Carstens et al. (1969) and the fixed bedform data of Bagnold (1946), Grant and Madsen (1982) found that the simple formula

$$k_b = 27.7\eta\left(\frac{\eta}{\lambda}\right) \tag{8}$$

produced good wave friction factor estimates when used in conjunction with their boundary layer model to compute the wave stress. The symbols η and λ denote ripple height and length, respectively. Nielsen (1992) found similar results but with a lower value for the coefficient. The Nielsen (1992) and Grant and Madsen (1982) type formulas are appropriate for noncohesive sands. In general, roughness is determined parametrically by running a stress model and adjusting the drag coefficient until the solution converges to data. The geometry of the bedforms is measured and then regressed against the modeled roughness to estimate the roughness coefficient.

3.1.2 Ripple geometry models

Equation 8 requires ripple geometry estimates, and a number of studies to relate ripple dimensions to wave conditions has been carried out. Conceptually, ripple geometry under waves is a function of the near-bottom wave, fluid and sediment characteristics. Written symbolically,

$$\eta,\lambda = f\left(D,\rho,\rho_s,g,A_b,u_b,\nu\right) \tag{9}$$

where D is sediment grain size, ρ is fluid density, ρ_s is sediment density, g is acceleration due to gravity, and ν is the kinematic viscosity of water. In terms of the momentum balance, the first four terms (D, ρ, ρ_s, g) represent the tendency for particles to settle or remain immobile, and the last three parameters (A_b, u_b, ν) represent the energy required to mobilize sediment, thus deforming the bed to create bedforms. Ripple geometry models generally express η and λ as a function of the wave and sediment characteristics with fitting coefficients derived from measurements.

Early work expressed the ripple dimensions as a function of the skin friction shear stress (Grant and Madsen 1982; Nielsen 1981), but as more data became available, it was found that ripple characteristics could be expressed in terms of the more easily measured wave parameters. For equilibrium ripples, in which ripples tend to grow with increasing wave orbital diameter and ripple steepness is constant, the following simple formula has been widely accepted:

$$\lambda = 12.4 A_b \qquad \frac{\eta}{\lambda} = 0.15 \tag{10}$$

where the numerical values show some variability in the literature. For stronger flows, the ripples were no longer in equilibrium with the waves and began to wash out. Under these conditions, Wiberg and Harris (1994) noted that ripple length was proportional to grain size ($\lambda = 535D$), and ripple steepness decreased with increasing flow intensity. They developed a parametric model that relates ripple steepness to wave orbital diameter under stronger flow conditions. Their analysis resulted in a ripple geometry model valid for a broad range of wave and sediment conditions, with wave orbital diameter and sediment grain size the only input parameters.

Wikramanayake and Madsen (1991) reviewed several nondimensional parameters commonly used in sediment transport studies and found that the ratio of the mobility number, θ_m,

$$\theta_m = \frac{u_b^2}{(s-1)gD} \tag{11}$$

and the nondimensional sediment parameter, S_*,

$$S_* = \frac{D}{4\nu}\left[(s-1)gD\right]^{1/2} \tag{12}$$

was well correlated to the ripple data of Inman (1957), Dingler and Inman (1976), and Nielsen (1984), where s is the relative sediment density (= ρ_s/ρ) Using these original data sets and the field data of Traykovski et al. (1999), Styles and Glenn (2002) revisited the Wikramanayake and Madsen (1991) model and produced the following empirical formula:

$$\frac{\eta}{A_b} = \begin{cases} 0.30\mathrm{X}^{-0.39} & \mathrm{X} < 2 \\ 0.45\mathrm{X}^{-0.90} & \mathrm{X} > 2 \end{cases}$$

$$\frac{\lambda}{A_b} = \begin{cases} 1.96\mathrm{X}^{-0.28} & \mathrm{X} < 2 \\ 2.71\mathrm{X}^{-0.75} & \mathrm{X} > 2 \end{cases} \tag{13}$$

where

$$\mathrm{X} = \frac{\theta_m}{S_*} = \frac{4\nu u_b^2}{D\left[(s-1)gD\right]^{1.5}} \tag{14}$$

Ripple geometry is written explicitly in terms of easily computed wave parameters making this model attractive for computing bedforms in coupled, bottom boundary layer/shelf circulation models.

Other equilibrium ripple models have been proposed, yet the basic underlying approach is to express bedform geometry in terms of either the sediment transport characteristics (i.e., the Shields initiation of sediment motion criteria or some other mobility function) or directly in terms of the near-bed wave parameters as discussed above. Van Rijn (2007a) gives a good review of previous studies including the range of wave and sediment conditions for applying equilibrium-type wave ripple formulas.

3.1.3 Time-evolution ripple models

In the last decade, studies have begun to focus on the nonequilibrium and time dependence of bedforms (Smith and Sleath 2005; Testik et al. 2005), whereas previous work treated them as quasi-steady. Doucette and O'Donoghue (2006) examined ripple evolution in response to changes in wave-generated flow in an experimental water tunnel at full-scale conditions. They conducted experiments with both initial flat beds and bedforms and noted that the equilibrium adjustment time was not sensitive to the initial bed configuration. Ripple evolution was sensitive to mobility number, and they presented a simple ripple adjustment model that predicted the time required to reach equilibrium.

Traykovski (2007) used field data to examine the evolution of ripples under changing forcing conditions including relic ripples. Their model expressed ripple dimensions as a function of the wave orbital diameter for equilibrium conditions similar as described above but included a time-dependent modification once a sediment transport threshold was reached based upon sediment grain diameter and wave characteristics. The time dependent model was a function of ripple cross-sectional area and sediment transport rate. The model allowed for exponential adjustment of ripple length between equilibrium events and was shown to accurately predict the long-wavelength relic ripples whereas the equilibrium model alone failed.

3.2 Wave and currents at arbitrary angles

Another research area that has received mixed attention is the role of waves and currents at arbitrary angles. Many laboratory studies are designed to examine wave transformations. As such, experimental facilities are constructed as long, rectangular flumes or oscillating water tunnels so that the aspect ratio is too small to generate crosscurrents.

In natural settings, the angle between the wave and current varies considerably, so field sites are tailored towards oblique angle studies. Drake et al. (1992) measured near-bed velocity profiles and waves on the northern California shelf to obtain estimates of shear stress and to validate existing bottom roughness formulations. They noted a directional dependence in bottom roughness and theorized a simple correction to established bottom roughness equations (Grant and Madsen 1982) to include the wave and current direction

$$k_b = 27.7\eta\left(\frac{\eta}{\lambda}\right) - 0.14\left(90 - \phi_{cw}\right) \tag{15}$$

For co-directional waves and currents, φ_{cw} = 0 and the correction term reduces the bottom roughness from a pure wave. When the wave and currents are orthogonal (φ_{cw} = 90), the roughness is slightly increased and equals estimates obtained for pure waves. Sorenson et al. (1995) found that the following correction to existing roughness formulations produced good agreement between field data and their bottom boundary layer model

$$k_b = 1.14\left[\cos\phi_{cw}\right]^{1.2} \tag{16}$$

Their correction implies a weakly nonlinear dependence on φ_{cw}. Using laboratory data from a rectangular basin with oblique waves and currents, You (1996) noted a weak dependence on wave direction using a combined flow model. However, he was unable to establish with statistical certainty a direct dependence, so his analysis led to a roughness formulation based upon wave parameters only without an explicit φ_{cw} dependence.

The two formulas predict widely varying corrections to the co-directional wave and current roughness formula (Equation 8) despite the fact that they are applicable to similar conditions (Figure 3). Drake et al. (1992) did note that their formula was calibrated from data collected during a single

deployment and that further investigation was necessary to determine its validity for a broader set of conditions. In any event, the disparate results provide evidence that a strong functional dependence on φ_{cw} has not been proven despite the fact that orthogonal waves and currents may possess different roughness characteristics, especially in the presence of heterogeneous bedforms.

Figure 3. Bottom roughness correction for waves and currents at arbitrary angles.

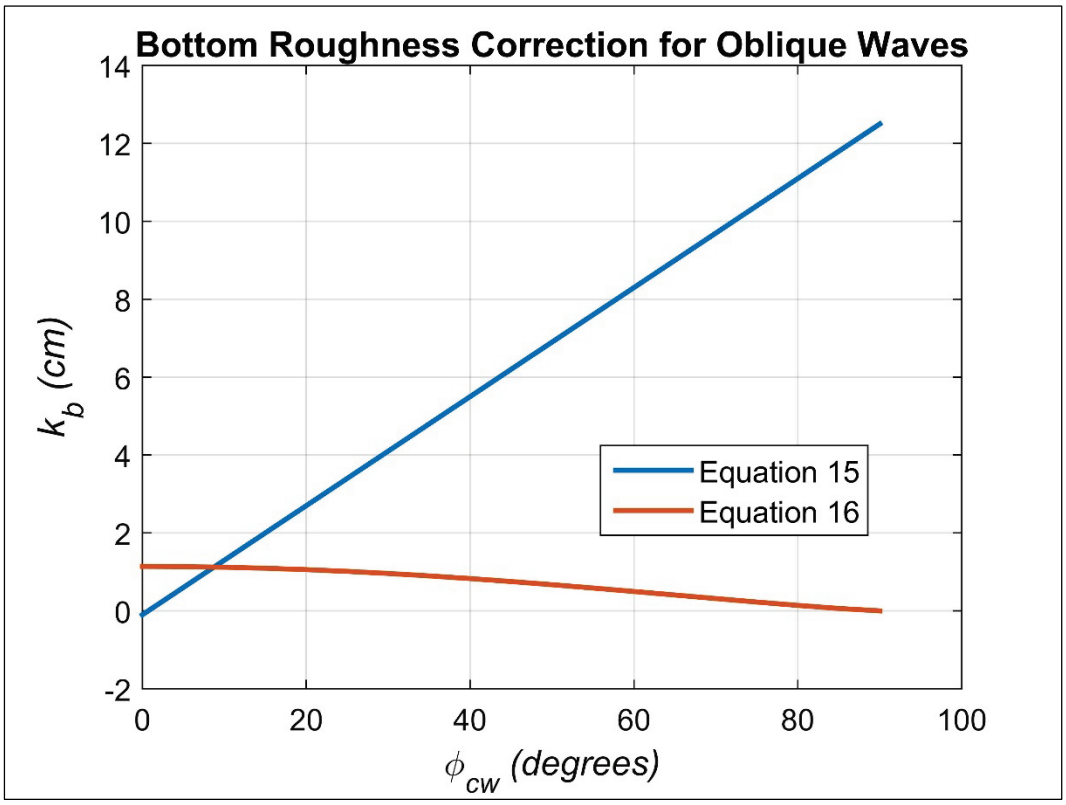

The above studies used regression analysis to compute shear stress from velocity profiles rather than direct covariance measurements. This is a common practice owing to the difficulty of measuring the bed stress directly. Past studies often lack the necessary instrumentation to measure both the bottom shear stress and bedform geometry with sufficient resolution to distinguish model sensitivity to oblique waves and currents.

Because waves and currents in natural environments are seldom co-directional, the total bottom stress depends on the angle between the wave and current. The maximum shear stress is the vector sum of the time-average of the instantaneous shear stress plus the maximum shear stress for the wave:

$$\vec{\tau}_{cw} = \vec{\tau}_c + \vec{\tau}_{wm} \tag{17}$$

where the arrow denotes a vector quantity. Writing Equation 17 in terms of the shear velocities gives

$$\vec{u}_{*cw} u_{*cw} = u_{*c}^2 \left(\cos\phi_{cw} \hat{i} + \sin\phi_{cw} \hat{j} \right) + u_{*wm}^2 \hat{i} \tag{18}$$

where $\hat{\imath}$ and $\hat{\jmath}$ are unit vectors in the x and y directions, respectively, and the general expression between stress and shear velocity ($\tau = \rho u_*^2$) has been invoked. Taking the magnitude of Equation 18 and rearranging gives the following equation for the relative maximum wave stress as a function of the relative current stress:

$$\frac{u_{*wm}^2}{u_{*cw}^2} = \left[1 + \left(\frac{u_{*c}}{u_{*wm}} \right)^2 \cos\phi_{cw} + \left(\frac{u_{*c}}{u_{*wm}} \right)^4 \right]^{-1/2} \tag{19}$$

As $u_{*c} \to 0$, the right-hand side approaches unity, and the combined stress is equal to the wave stress. As the ratio of the current stress to wave stress increases, the right-hand side becomes small, and the relative contribution from the wave is minimal. When $\varphi_{cw} = 0$, the contribution from the current stress to the total starts to become significant when $u^2_{*c}/u^2_{*wm} > 0.2$ (Figure 4). When $\varphi_{cw} = 90$, this same level of contribution occurs for $u^2_{*c}/u^2_{*wm} > 0.56$. Even when the wave and current stress components are orthogonal, the current still affects the wave as long as u_{*c}/u_{*wm} remains finite. The shear velocities define the eddy viscosity, which shapes the velocity and concentration profiles, and the boundary layer thickness. The body of knowledge detailing the fine structure of combined wave and current boundary layers is limited owing to the difficulty of creating controlled wave conditions with free crosscurrents and to the lack of resources to resolve the vertical structure on the millimeter scale. Combined flow studies are needed to establish the validity of the theoretical models that assume nonlinear coupling is important for wave and current angles near 90 degrees.

Figure 4. Contour plot depicting the relative wave stress (u^2_{*wm}/u^2_{*cw}) as a function of the angle between the wave and current.

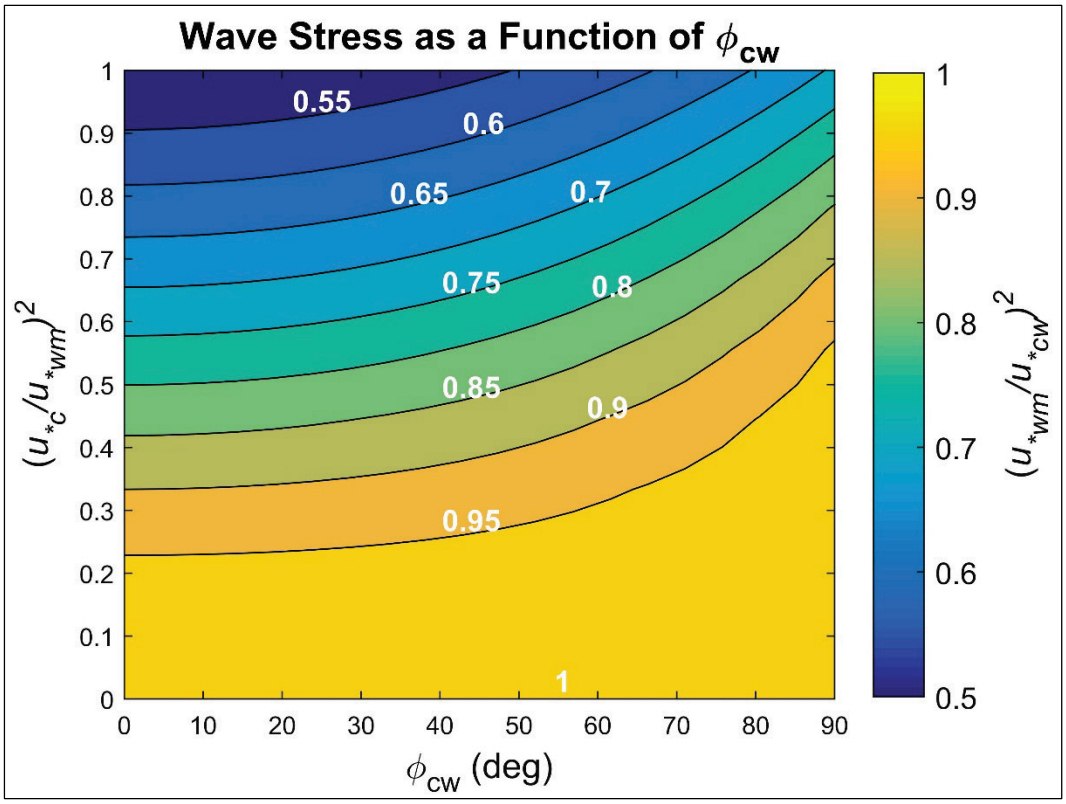

3.3 Eddy viscosity closure

Eddy viscosity models are widely used to represent the turbulence Reynolds fluxes in combined wave and current flows. Eddy viscosity closure methods lead to analytical solutions, which permit deeper insight into the functional relationship between boundary layer variables. For neutral conditions, Lynch et al. (1997) identified a transition layer near the top of the wave boundary layer in their suspended sediment concentration measurements that was not consistent with previous eddy viscosity formulations adopted by Grant and Madsen (1979) and Glenn and Grant (1987). They showed that the Wikramanayake and Madsen (1992) continuous eddy viscosity model accurately predicted the cutoff point identifying the edge of the transition layer and was more accurate than the Grant and Madsen (1979) discontinuous eddy viscosity model. For stratified flows, the functional form of the correction to the eddy viscosity originally suggested by Businger et al. (1971), who developed their eddy viscosity for thermally stratified atmospheric boundary layers, was shown to be valid for suspended sediment-induced stratification by Villaret and Trowbridge (1991).

3.3.1 Eddy viscosity for stratified fluids

The eddy viscosity models of Glenn and Grant (1987) and Styles and Glenn (2000) include a correction to account for suspended sediment-induced stratification for the flow

$$K_{strat} = \frac{K}{1 + \beta \frac{z}{L}} \tag{20}$$

and for the concentration

$$K_{s\,strat} = \frac{K}{\gamma + \beta \frac{z}{L}} \tag{21}$$

where β and γ are empirically derived constants and z/L is the stability parameter. The modified eddy viscosities are applied to either Equation 1 or Equation 2, and the velocity and wave solutions are solved iteratively with a coupled sediment concentration model. Because the stability parameter is in the denominator, the stratified eddy viscosity is smaller than the neutral version. Stratification decreases the magnitude of turbulent fluctuations as the upward fluid velocity must overcome gravity in the stratified layer. These fluctuations are responsible for turbulence transport, and when they are reduced, so is the vertical momentum and mass flux.

The eddy viscosity is a function of the vertical coordinate and the Monin-Obukov length (L) through the stability parameter. The Monin-Obukov length is defined as

$$L = \frac{u_*^3 \rho}{\kappa g \theta_*} \tag{22}$$

where θ_* represents the vertical turbulence flux of the stratifying medium (Stull 1988). In the atmosphere, θ_* is a function of density fluctuations due to temperature gradients, but in the bottom boundary layer, it is due to vertical gradients in sediment concentration. Physically, L is a measure of the relative turbulence transport of momentum to turbulence transport of mass in the near-bed surface layer. As L increases, turbulence transport of momentum dominates mass transport, and the effects of stratification are

reduced. Equation 22 is for the surface layer in which the length is assumed constant. However, momentum and mass fluxes can vary in the near-bed region as the stress terms are reduced in the outer wave boundary layer. The stability parameter can increase or decrease with height depending on changes in concentration and stratification. The eddy viscosity is sensitive to the vertical structure of L (Figure 5) and shows significant differences from neutral conditions. Further from the bed, L eventually becomes infinite once the stresses are too weak to maintain sediment in suspension, and the stratified eddy viscosity relaxes to the neutral profile.

Figure 5. Stratified eddy viscosity profile. The primes denote nondimensional variables. The limiting case of a neutral boundary layer and associated linearly increasing eddy viscosity is illustrated for comparison.

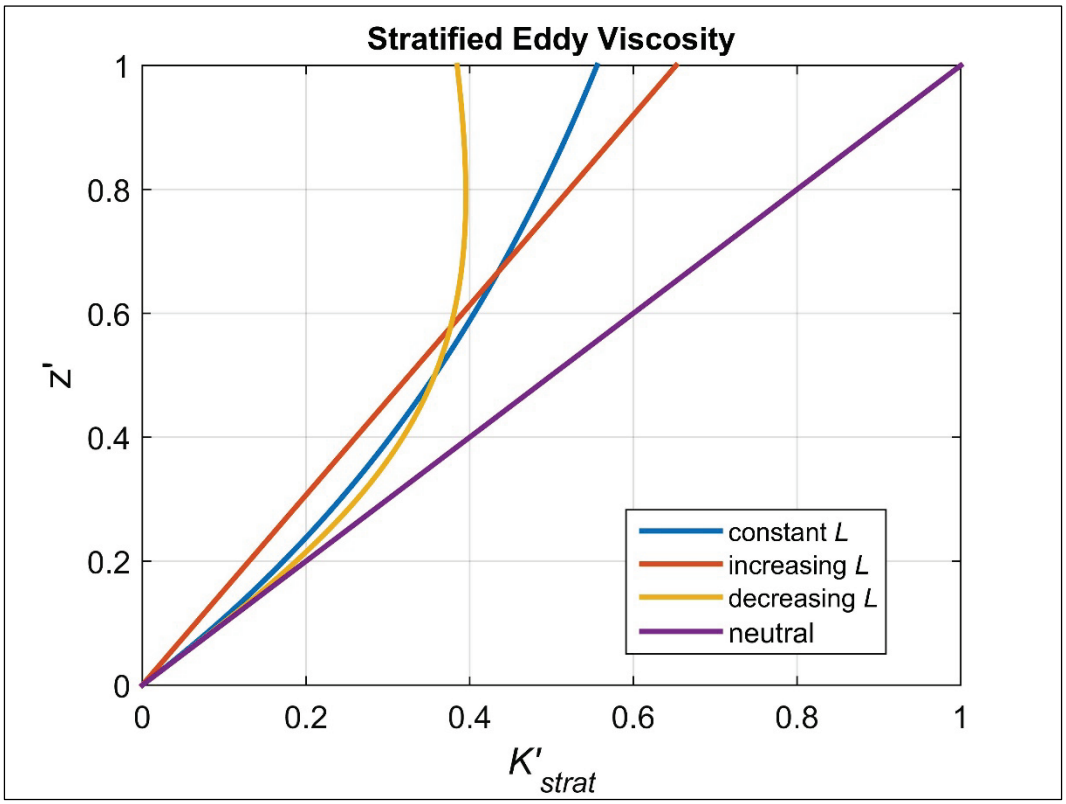

Equations 20 and 21 have not been widely validated in the field or laboratory. Both models assume that stratification occurs under very high sediment concentrations and affects only a thin layer within the lower boundary layer. The stratified model predicts negatively skewed velocity and concentration profiles with increased shear within the stratified layer. For noncohesive sediments, this requires energetic wave and current conditions and fine-scale measurements within the wave boundary layer to distinguish the velocity and concentration profiles form neutral conditions.

For cohesive sediments, suspended sediment-induced stratification is likewise important, but there have been no studies to validate analytical models that incorporate suspended sediment-induced stratification.

Progress towards developing better parameterizations to represent the turbulent fluxes of mass and momentum in models requires direct estimate of these fluxes under a variety of wave and current conditions. The demonstrated sensitivity of the eddy viscosity to surface fluxes through L and the underlying assumption that Monin-Obukov similarity derived from atmospheric boundary layers is appropriate for oceanic boundary layers needs to be reconciled with observations, and if necessary, rejected and replaced with new approaches. For example, surface fluxes, which Monin-Obukov similarity is based, may not be appropriate farther from the bed where turbulence intensity is reduced. In this case, local fluxes are more appropriate to scale the variables and define the relevant length scales.

3.3.2 Time-dependent eddy viscosities

Wave streaming caused by asymmetry over the wave cycle and nonlinear effects has been shown to be an important factor for sediment transport. Early models of wave boundary layers used time-varying eddy viscosities to investigate the nonlinear behavior of real ocean waves. Trowbridge and Madsen (1984) formulated a time-dependent eddy viscosity as a set of Fourier modes resulting in multiple harmonics in the solution that led to a slow, steady streaming near the bed. For longer waves, the streaming reversed direction to flow in the opposite direction of wave propagation. Foster et al. (1999) also developed an analytical time-varying eddy viscosity model to examine cross-shore wave transformations. They showed good agreement between their model and previously reported laboratory data. For skewed waves, the net stress was directed onshore, and for purely asymmetric waves, it was direction offshore.

Time-varying eddy viscosities permit multiple vertical modes leading to more realistic streaming associated with real ocean waves. However, the above studies did not consider the combined flow case as it was assumed that the waves dominate the current. The magnitude and direction of streaming is a function of wave asymmetry, bottom stress, and bed roughness conditions and is a principal consideration in developing accurate sediment transport models. The supplemental effect of oblique currents is virtually unexplored in time-dependent eddy viscosity

formulations, and a theoretical treatment with supporting measurements is needed. Furthermore, these methods were applied to waves propagating over flat beds. The case for sloping beds has not been explored except in the potential flow region outside the wave boundary layer.

3.4 Near-shore wave transformations

Energy transformations across the littoral zone represent complex fluid dynamical processes in coastal regions. Near-shore sediment transport driven by waves and currents helps control beach morphology and longshore bar maintenance and evolution. In the present context, the domain of interest extends between the inner shelf, where the bed slope is very mild and the seabed can be treated as horizontal, to the edge of the breaker zone, where waves are on the cusp of breaking but still have not yet begun to spill over. Within this region, linear wave theory predicts abrupt changes in wave height characteristics (Figure 6). Once the water depth is on the order of a few meters, wave height reduces slightly but then grows rapidly as the energy is confined to an increasingly compressed water column. Kinetic energy distributed along the wavelength is converted into potential energy causing wave growth. Eventually, wave steepness reaches a critical point, and the fluid velocity overtakes the wave celerity, and instabilities arise in the form of wave breaking.

Linear theory predicts equal current magnitudes during both halves of the wave cycle so that net transport is zero under a progressive wave. Real progressive waves produce a net streaming in the direction of wave propagation termed *Stokes drift*. Stokes drift is a consequence of mass conservation and vertical shear as the water column is deeper under the crest and shallower under the trough, leading to slightly higher maximum currents under the crest. In addition to Stokes drift, it has long been known that progressive waves generate a net flow owing to nonlinearities inherent in damped harmonic systems. Longuet-Higgins (1953) showed theoretically that phase shifts in the flow velocity induced by friction led to steady streaming in the wave boundary layer. As mentioned above, the work of Trowbridge and Madsen (1984) showed that nonlinear bottom friction leads to asymmetries in maximum shear stress creating drift velocities in the wave boundary layer over flat beds. The net flow either progresses with the wave, as in Stokes drift, or offshore due to velocity-skewness, which can dominate for longer waves. The drift velocity is characteristic of waves propagating over flat beds, but shoaling can enhance wave asymmetry producing more complex streaming.

Figure 6. Shallow water wave height transformation as a function of period (*T*). The predictions are derived using linear wave theory. Waves will begin to break once the wave-induced oscillatory water motion exceeds the wave phase speed.

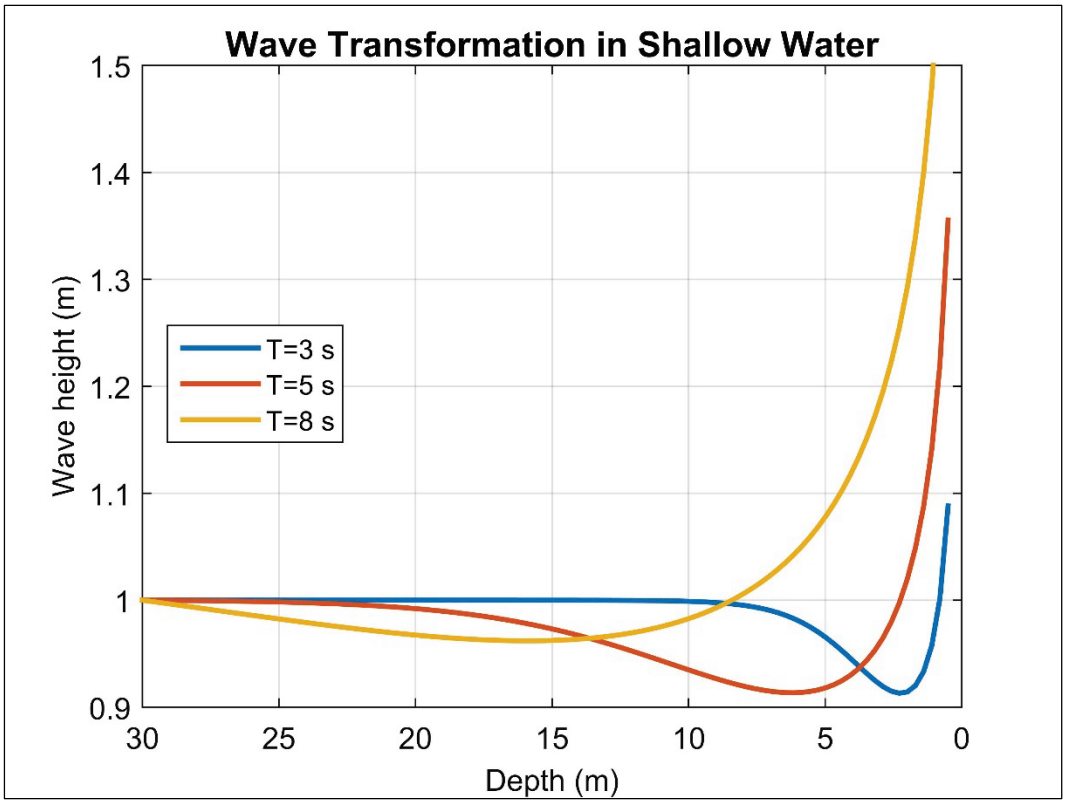

Kranenburg et al. (2012) investigated the effect of wave shape on streaming using a 1D numerical model over a flat but very rough bed. The momentum equation was closed using a q-ε turbulence closure method permitting time variation in the stress and eddy viscosity. The model was validated using laboratory data from two flumes and two water tunnels ranging in length from 10 to 46 m and width from 0.3 to 1.0 m. Velocity and phase profiles were measured within the wave boundary layer down to the millimeter scale. They determined that the wave-streaming velocity was a function of the relative bottom roughness and relative water depth. For decreasing water depth, wave-shape induced streaming begins to dominate over progressive wave streaming. Increases in relative roughness tend to show a shift towards onshore streaming.

Waves traveling into shallow water tend to develop asymmetries in profile shape that lead to different maximum velocities under the crest and trough. The wave form develops a skewed appearance with the forward slope compressed into a steeper angle and the trailing slope elongated into a shallower angle. Forward velocities under the crest accelerate faster and

reach a higher maximum velocity compared to the trough. From the potential flow region, this asymmetry penetrates to the bottom, essentially leading to asymmetrical forcing of the wave boundary layer. This in turn drives asymmetries in maximum bottom shear stress and associated currents leading to steady streaming that is a direct result of shoaling and friction.

Past studies have investigated the behavior of waves propagating over a sloping bottom. Like a flat bed, potential theory predicts wave asymmetries and associated streaming over a mildly sloping bed without invoking frictional effects (Chu and Mei 1970). Zou and Hay (2003) developed a theoretical model of wave propagation over a sloping bed. While their solution for the potential flow region followed the Chu and Mei (1970) inviscid theory, the wave boundary layer solution was equivalent to the flat-bed case. They assumed that the effect on the wave boundary layer could be incorporated through the steady streaming associated with the potential flow. Turbulence closure was achieved using both an eddy-viscosity and a viscoelastic-diffusion model. They compared their model with measurements obtained over a sloping beach and showed good comparison with velocities and shear stress profiles. Owing to the small aspect ratio, the sloping bed had a strong influence on vertical velocities but not on horizontal velocities or bed shear stress.

Berni et al. (2013) studied wave characteristics using a physical model of a beach in a two-dimensional (2D) wave flume. Their facility consisted of a 36 m long by 0.55 m deep flume constructed with a sediment beach of 0.64 mm sand. They measured velocity profiles in 3 mm increments from the bed up to the free-stream level at a distance of 13 m from the wave maker. They found a linear relationship between the free-stream velocity asymmetry and the bottom velocity skewness with an approximate 40 degree phase lead. They suggested that it may be possible to estimate bottom velocity from free-stream velocity using their formula. However, their experiments were carried out under transforming waves at a single cross-shore location (water depth) on the sloping beach without a crosscurrent. Another approach would be to generate constant offshore waves and vary the depth of the sensor by placing it at several cross-shore locations under the same wave and current forcing. In this way, it would be possible to measure the wave transformation directly as it propagates across a sloping bed with the more realistic case of a steady alongshore current.

Wilson et al. (2014) measured bottom shear stress over a steeply sloping beach in Nova Scotia, Canada, over a mixed sand-gravel beach with sediments ranging from coarse sand to cobbles. Profiles were obtained over the lower 20 cm of the water column at a point near midtide so the instruments were exposed during low tide. They measured the ambient flow and deployed a fan-beam and a pencil-beam sonar to measure bedforms. They reported time series and vertical profiles of the Reynolds stress in the context of the effects of a sloping seabed and bedforms. They showed good agreement between their dissipation measurements with the theoretical model of Zou et al. (2003) and noted that outside the wave boundary layer, the majority of variability in the stresses was due to bed slope. However, they noted that as wave height increased, the measurements did not in general agree with the theory within the wave boundary layer.

3.5 Wave-induced longshore currents

Gradients in the radiation stress are caused by breaking waves propagating at oblique angles to the shoreline generate longshore currents. Because the large gradients are generated by breaking, the majority of the current is confined to the breaker zone and decays rapidly offshore due to gradient diffusion. Longuet-Higgins (1970) developed one of the earlier theoretical models by assuming that the longshore current (U_L) is driven by a balance between wave radiation stress and friction:

$$U_L = \frac{5\pi}{8}\frac{\delta S}{C_f}\sqrt{g h_b}\sin\phi_b\cos\phi_b \tag{23}$$

where S is bottom slope, C_f is a dimensionless friction coefficient, h_b is the water depth at breaking, φ_b is wave angle (measured from shore normal) at breaking, and δ is a parameter that accounts for wave setup and is defined as

$$\delta = \frac{1}{1+\frac{3H_b^2}{8h^2}} \tag{24}$$

The longshore current increases with beach slope and shallow-water phase speed, such that higher wave heights at breaking (H_b) produce stronger currents. The parameter δ indicates that waves breaking in deeper water contribute to stronger currents, so the combination of higher waves

breaking farther from shore effectively widens the surfzone to produce the strongest longshore currents. Noting that the phase speed at the breaking point can be expressed in terms of wave height, Komar (1975) derived a simpler expression:

$$U_L = 1.0\sqrt{gH_b}\sin\phi_b\cos\phi_b \tag{25}$$

Komar (1975) demonstrated that Equation 25 produced good estimates of the current for angles up to 45 degrees when compared to available lab and field data.

Longuet-Higgins (1970) also developed equations to predict the cross-shore variation in the current. The no-slip condition at the coast produces a lateral shear layer that increases offshore to a maximum between 0.5 and 0.75 times the point of breaking waves. The current then decays offshore due to gradient diffusion to a point approximately two times the breaker point. The profile can be described as quasi parabolic that is skewed slightly offshore; thus, the strongest currents occur between the breaker point and shoreline.

Dalrymple and Liu (1978) examined theoretically the cross-shore current profile by examining the drag induced by waves and currents but did not include lateral mixing, whereas Madsen et al. (1978) and Kraus and Sasaki (1979) formulated their stress term to include mixing. The first comparison between the existing theories and measured profiles was conducted by Kraus and Sasaki (1979) using data obtained in the near-shore region at Urahama Beach in Japan. The models showed good agreement in the outer breaker zone and offshore but were less accurate in the near-shore zone as the theoretical assumptions of constant wave height did not hold. Other investigators have included more realistic conditions including random wave fields and spectral decomposition as in the case of locally generated waves in the presence of distant swell (Guza et al. 1986; Thornton and Guza 1986). Because of the complexity of real beaches, the majority of analytical treatments are limited to simplified geometries consisting of uniform beach slopes and straight and parallel longshore contours.

Real beaches generally include cusps and other topographic features that produce longshore variability. Some beaches likewise possess multiple bar systems and associated complex wave transformation processes requiring numerical models to obtain quantitative predictions. Larson and Kraus

(1991) produced one of the early numerical models of wave-driven, alongshore currents. Their model was driven with offshore waves at arbitrary angles and produced estimates of the average longshore current, wave height, wave direction, and water elevation across the surf zone. The model showed reasonable agreement with available laboratory and field data (see Komar [1998] for details).

Since this early work, state-of-the-art numerical models have been developed specifically tailored toward the wave and current processes in the transition region across the inner shelf. Chen et al. (2014) developed a hybrid, near-shore wave, current, and sediment transport model for applications to the coastal zone. The model includes a coupled version of SWAN to compute waves along with the sediment transport models of Kobayashi et al. (2008), Soulsby (1997), and Van Rijn et al. (2011). The first sediment transport model includes wave-induced, cross-shore sediment transport and is designed for beach profile evolution while the second includes total current transport driven by waves and the third includes transport due to wave asymmetry. The primary validation conditions were for beach profiles and sand bar migration, which place the calibrations near the edge and within the breaker zone. They noted the sediment transport formulas were more accurate during energetic events but less so during low-energy events and that more data are needed to further improve the sediment transport models.

The above studies are primarily aimed at longshore currents landward of the breaking point; however, the theories also predict the decay in current offshore due to shear-induced mixing. Tides, winds, long waves, and alongshore setup also contribute to longshore currents. These currents extend beyond the breaker zone and interact with the shoaling waves nonlinearly, yet very little is known about wave-current interaction due to the scarcity of observations.

4 Fine-Grained Transport and Viscoelastic Beds

4.1 Cohesive sediment transport theory

Beds consisting of fine-grained material (mud) behave very differently from noncohesive sands when acted upon by an applied stress as generated by waves and currents (Mehta et al. 1989; Winterwerp and Van Kesteren 2004). Fine-grained material in a heavily concentrated fluid mixture forms cohesive deposits that tend to behave more like an elastic medium as opposed to a viscous fluid (Ng and Zhang 2007). Experimental results show that a highly consolidated cohesive bed acted upon by waves can behave very non-Newtonian (Maa and Mehta 1988) and has been the impetus for investigating wave propagation over muddy beds by treating the bottom as a hybrid viscoelastic surface (Dalrymple and Liu 1978; Foda et al. 1993; Jain and Mehta 2009; Mallard and Dalrymple 1977; Mei et al. 2010; Ng and Zhang 2007; Soltanpour et al. 2009). This approach simplifies the dynamics as the total bottom shear stress is the algebraic sum of two terms representing the local strain rate and the elastic modulus. Wave damping is controlled by a combination of linear friction and vertical deformation of the quasi-elastic seabed. The additional energy loss leads to greater wave attenuation over a mud bed compared to a fixed bed.

Conceptually, the boundary layer is depicted as a two-layer system consisting of a highly concentrated mud layer separated by an overlying sediment-free water column. As such, layer thickness and rheological characteristics are as equally important as the waves, currents, and sediment properties for investigating the physical behavior of mud bottoms. Studies have progressed through the years to include more realistic mud properties as new information on cohesive sediment emerges.

Dalrymple and Liu (1978) developed a theoretical model of wave propagation above a mud bottom. Their approach consisted of a two-layer system with a sediment-free water column overlaying a mud layer of arbitrary thickness. The momentum and mass conservation equations were solved independently within each layer, and matching boundary conditions at the interface allowed the mud layer to respond dynamically to the waves. In order to model the cohesive properties of the mud layer, they treated the

lower layer as a highly viscous fluid permitting an eddy-viscosity closure. The solution included wave damping and vertical profiles of the current, pressure, and phase as a function of layer thickness and wave parameters. They noted good agreement between the damping coefficient and wave number as a function of layer thickness with available measurements.

Foda et al. (1993) developed a two-layer model similar to the conceptual design of Dalrymple and Liu (1978) but treated the mud layer as a nonlinear viscoelastic medium. The stress term within the lower layer included a correction to account for the viscoelastic properties of the mud layer. Their theoretical solution led to predictions of the fluidized layer thickness as a function of the wave and rheological characteristics of the sediment. Wave attenuation tended to increase as a function of the layer thickness and bed stiffness. Foda et al. (1993) further surmised that the mud behaved like an elastic solid for relatively low strain amplitude and a viscous fluid under a high strain amplitude. In between, the mud demonstrated both viscous and elastic characteristics.

Ng (2000) developed a theoretical model of waves propagating over a mud bed to examine Stokes-induced transport. He assumed that the boundary layer thickness, wave amplitude, mud depth were comparable but much less than the wavelength, permitting boundary layer scaling to simplify the governing equations. The analytical solution predicted wave damping rate to first order and mass transport velocity of the mud to second order, allowing a detailed analysis of the vertical flow structure including flow asymmetries. As in previous studies, wave damping was a function of mud-layer depth, with a peak damping rate at a relative mud depth of 1.5. Mass transport increased with layer thickness but decreased with mud density as the heavier material was more sluggish and had weaker accelerations. The results also indicated a sharp gradient at the interface in mass transport velocity, with much higher transport outside the mud layer. In real flows, the transition is smoother, so as sediment is lifted higher off of the bed, it encounters much stronger flows with greater transport potential.

Mei et al. (2010) studied the interaction of water waves and a mud bottom theoretically using a two-layer model that treated the mud as a viscoelastic material with a frequency-dependent complex viscosity. The overlying water column was assumed inviscid and driven by small amplitude waves with a narrow frequency band. Over long distances, wave attenuation and

dispersion characteristics were modified due to the presence of the mud bottom. For thick mud layers and strong elastic properties, they found that mud motion could be significantly modulated through resonant interactions between wave frequency and rate of deformation. This could have implications for dislodging bottom sediment and initiation of sediment motion. Dispersion characteristics between first- and second-order wave modes led to asymmetries in damping that generated current reversals that strengthened over distance.

4.2 Laboratory studies

Sakakiyama and Byker (1989) investigated theoretically and experimentally the mass transport of fine-grained sediment under waves. The experimental setup included a rectangular wave basin (24.5 m long, 0.57 m deep, 0.5 m wide) driven by a paddle-type wave maker. The 12 m long test section had a 0.095 m deep recess containing a mixture of kaolinite and water. Twenty-one test cases were reported with wave heights ranging from 0.01 to 0.044 m and periods from 0.6 to 2.0 s. Mud transport rate was proportional to stress but with a higher power than the square of the wave height, which has been reported for noncohesive sediments (Nielsen 1992). They attribute this to the nonlinear relationship between stress and strain owing to the weakly nonelastic properties of mud.

De Wit and Kranenburg (1996) conducted flume experiments to investigate liquification of mud in a combined wave and current flow. The flume dimensions were 40 m long by 0.8 m wide by 0.8 m deep with an 8 m long test section containing a 0.2 m thick layer of clay. The experiments were designed to induce liquification and collect velocity and concentration profiles within and above the liquefied layer. Wave damping began once the fluid layer formed and increased as a function of layer depth. Measured velocity profiles showed sharp gradients at the interface and generally agreed well with a two-layer wave model. Very little fluid mud was transported by the current. They attributed this to the flume design, which hindered flow at the end of the flume, and the high viscosity of the fluid mud, which prevented resuspension, thereby limiting the concentrations to the lower boundary layer where currents are weak.

Lamb et al. (2004) conducted laboratory experiments to investigate boundary layer dynamics with high concentrations of fine-grained sediments under waves. The experimental setup consisted of an oscillating U-tube to simulate wave motion and a 0.2 m wide by 4.9 m long by 1.2 m

deep working section. The false bottom was replaced with a 10 to 15 cm thick sediment bed consisting of ~ 20 μm particles. Concentrations ranged between 17 and 80 g/L, and a lutocline formed separating the upper water column from the high-concentration, near-bed layer. Wave boundary layer thickness without sediments was on the order of 1 cm but then reduced to < 0.3 cm when sediments were introduced. They surmised that the reduced boundary layer thickness was due to sediment-induced stratification, as the energy required to generate and maintain the stratified layer reduced the turbulence kinetic energy available for the upward flux of momentum.

Zhao et al. (2006) conducted numerical and laboratory studies of fluid mud to better constrain and understand the processes controlling cohesive sediment transport in coastal areas. They used a similar approach as discussed above to close the momentum equation for the bottom shear stress and included wave and current interaction for co-directional flow. Their laboratory results were conducted in a 32 m long by 0.5 m wide by 0.6 m flume with a 9 m long movable-bed working section consisting of mud with a density between 1.10 to 1.4 g/cm^2. Wave height decay rate was an order of magnitude greater over the mud bed as opposed to the fixed bed. The rheological characteristics of muddy bed layers varied with water concentration such that the lower compacted layers were more elastic and the upper fluidized layers were more viscous.

4.3 Bottom roughness

Bottom roughness for fine-grained cohesive sediment is a function of the sediment grain size. In natural environments, the surface sediment layer contains a range of grain sizes such that bottom roughness is determined from a statistical distribution. Often, the bottom roughness is written in terms of a representative grain diameter (D50):

$$k_b = 2D_{50} \tag{26}$$

where "50" denotes the median grain diameter. The coefficient and choice of grain size statistic (D85, D90, etc.) vary somewhat, but the general linear relationship has been widely adopted in process studies and models (Winterwerp and Van Kesteren 2004).

Fine-grained sediments can form concentrations of fluid mud under the action of shear stresses generated by waves and currents. If the

concentrations are high enough, a thin layer forms separating the outer fluid from the denser mud layer producing suspended sediment-induced stratification. Stratification inhibits the upward flux of turbulence, reducing vertical shear and flow velocities within the concentrated layer. Outside the layer, stratification is negligible, and the current shear is increased. Bottom roughness defined in terms of grain size will overpredict the magnitude of the current at the mud-water interface and within the concentrated layer.

The vertical flow structure and associated transport is more accurately modeled when the bottom roughness is defined in terms of the thickness of the concentrated layer. Layer thickness is proportional to the shear stress, which is a function of the physical bottom roughness, producing a positive feedback requiring a procedure to formulate a closed equilibrium solution.

Wilson (1989) found that the roughness due to sheet flow (k_t) was linearly proportional to the Shield parameter (Ψ):

$$k_t = 5D\Psi = \frac{5\left|\tau_b'\right|}{\rho(s-1)g} \tag{27}$$

where $\left|\tau_b'\right|$ is the magnitude of the skin friction shear stress. Adopting a drag coefficient to close the stress term (see Wilson [1989] for details) gives

$$k_t = 0.0655\left(\frac{u_b^2}{(s-1)gA_b}\right)^{1.4} \tag{28}$$

Equation 28 expresses the roughness due to sheet flow in terms of easily measurable wave parameters. Furthermore, theoretical studies note that the mud-layer thickness is a function of the wave height or, through linear wave transformation, u_b and A_b. Roughness length computed using Equation 28 is depicted in Figure 7. For typical values under strong flow conditions (u_b = 50-100 cm/s; A_b 100-150 cm), k_t is on the order of 10 to 40 μm. This is the same as grain roughness for sizes on the order of 5 to 20 μm without a sediment transport layer (Equation 26).

Figure 7. Bottom roughness predicted using Equation 28.

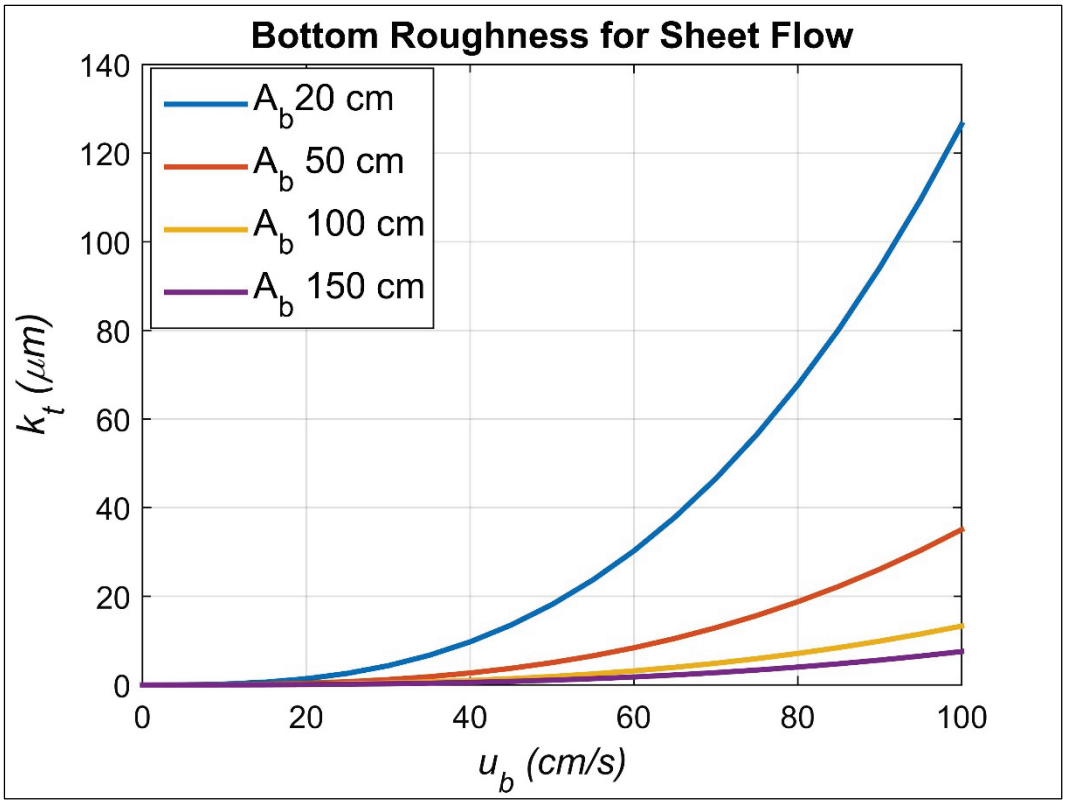

Bottom stress and associated roughness for muddy beds remain active research areas. Progress towards developing and testing empirical relationships and resulting numerical formulas to improve forecasting capabilities requires detailed sediment concentration, wave, current, and layer thickness measurements under a variety of forcing conditions. This includes direct measurements to separate the wave, turbulence, and current components to delineate and compute the Reynolds stresses, current profiles, and other turbulence statistics (e.g., production, dissipation, dispersion), which form the bases of theoretical formulas of key boundary layer processes.

5 Research Gaps

While wave and current studies abound in both the field and the laboratory, the majority focus on sandy sediment transport with co-directional waves and currents. Most cases that have considered wave and currents at arbitrary angles were conducted in the field, where it is difficult to control variables and measure the detailed near-bed flow structure (mm scale). Furthermore, fine-grained sediment transport has received more attention in the last few decades, but there is still a need to understand the role of suspended sediment-induced stratification and the mechanisms of sediment transport in combined flows. Bottom boundary layer models are designed for waves and currents at arbitrary angles and include sediment transport algorithms for a broad range of size classes including cohesive and noncohesive sediments. A deeper understanding of fine-grained sediment dynamics in combined wave and current flows is required to develop new algorithms that can expand model capabilities.

5.1 Research objectives

To this end, this review has identified several knowledge gaps in understanding fundamental physical processes, namely, the cross-shore transformation of waves and fine-grained sediment transport and how this is modulated in the presence of longshore currents. Several key research questions to address these issues and to make progress towards better predictive capabilities include the following.

Effect of oblique waves and currents – Studies have been conducted for waves and currents at oblique angles, but there still exists a need to explore the high-angle case for a wide range of relative wave and current conditions including the limit of pure waves and pure currents. How is the mass flux, turbulence stresses, and kinematics (i.e., velocity profiles) modified from the co-directional case and as the relative strength of the waves and currents change? How does the combined system respond for regular and irregular wave fields? Under what relative wave and current conditions is a representative wave (root-mean-square [rms], equivalent, significant, etc.) appropriate as opposed to the details of the time dependent wave field?

Effect of wave asymmetry in combined flows – Similar to the oblique case with symmetric waves, wave asymmetry introduces skewness in the wave velocity profile and associated mass flux and bottom shear stress. How does the asymmetry between the first and second half of the wave cycle interact with the oblique current to modulate the total bed shear stress as well as vertical distribution of the turbulence within the wave boundary layer?

Effect of wave transition into shallow water – While many studies have been conducted on wave and current boundary layer dynamics over a flat seabed, the transition between shallow water and the edge of the breaker zone is not well understood. The change in water depth produces gradients in momentum flux as the wave height and skewness increase over relatively short horizontal distances. Furthermore, the alongshore current profile is modulated as the water depth changes and the waves become more asymmetrical. How do gradients in the wave characteristics affect bottom stress, mass flux, and turbulence in the presence of an oblique and spatially varying current? How are the dynamics altered as the relative strength of the wave and current is manipulated?

Waves and currents over a mud bottom – Wave and current characteristics over a mud bottom are markedly different than over a noncohesive or flat bed. The weakly nonelastic properties of fine-grained sediments leads to greater energy loss and associated damping of the wave height. Furthermore, suspended sediment-induced stratification is a principal artifact of high concentration cohesive material and suppresses the upward turbulence flux resulting in sharp gradients in concentration and velocity profiles. How does the presence of oblique currents affect turbulence transport within the bottom boundary layer? What are the primary factors controlling sediment transport and stratification? Is there a defined threshold defining the stratification limit, and how is it modulated by wave and current conditions?

Testing and validating established combined flow models under the above conditions – Model validation requires high-resolution measurements of key variables to produce robust statistics, especially for complex nonlinear systems in which flow, turbulence, bedforms, and sediment transport are inextricably linked. State-of-the-art bottom boundary layer models need to be vetted for combined flows over mud bottoms to identify areas in need of improvement and to develop new algorithms to simulate these previously neglected processes. Can existing

models accurately reproduce the sediment, wave, and current profiles under combined forcing, and if not, what are their limits, and what new approaches are required to obtain accurate predictions?

5.2 Experimental program

Addressing the above objectives requires field and laboratory measurements to identify and quantify the contributing dynamic variables. Measurements include (1) direct covariance estimates of the Reynolds stress at different distances from the bed, (2) vertical shear to quantify turbulence kinetic energy production and dissipation as well as vertical water column structure, (3) sediment concentration within the bed and the water column including wave and turbulence fluctuations to define diffusion coefficients, (4) bedform geometry and evolution to relate stress to bottom roughness, and (5) high vertical resolution of the 3D current and waves to examine flow kinematics and to define empirical relationships.

Given the lack of knowledge of fine-grained sediment dynamics in combined flows, the data need to be collected in a way to ensure repeatability and continuity. This is an essential first step when constructing new formulations that must include a mechanism to assign metrics to gauge range of applicability. Laboratory conditions provide the control to ensure the repeatability needed to construct a robust statistical base for model validation. Once a model has been validated in the laboratory, the next step is to apply to the field. Field studies offer a full range of conditions including tides, storms, and stratification to validate and refine models. Ultimately, the goal is to improve computational tools to support a wide array of engineering applications.

5.3 Example calculations to determine range of laboratory inputs

Laboratory studies generally consist of flumes, tunnels, or basins at reduced scales compared to field settings. While some facilities house large flumes, the majority of experiments are limited in depth and width. Typical depths are on the order of a few meters at most, restricting wave heights to less than 1 m. Water depth is on the order of 1 m, but in many instances, it is less than half that, further restricting waves heights to a few tens of centimeters. As most flumes are designed to examine wave transformations, the widths are on the order of a few meters while the length can be on the order of tens of meters.

Studies designed to look at a range of flow conditions are required to develop formulas and algorithms to represent those conditions in models. The range of flow conditions available in the laboratory is limited by the dimensions of the facility. This places constraints on the magnitude of the variables of interest. Near-bed processes are driven by the ambient wave and current conditions, and the appropriate boundary layer parameters include the bottom orbital velocity and excursion amplitude. These can be derived from linear wave theory, which can be used to back calculate the wave height and wave period. This in turn defines the range of possible wave conditions available in a laboratory setting.

Assuming most laboratories restrict water depths to less than 1 m and wave heights to less than 0.25 m, linear wave theory predicts u_b ranges from 7 cm/s to 120 cm/s (Figure 8). This is a fairly broad range indicating that typical facilities encompass many different scenarios and thus provide robust statistics for validating formulas and algorithms. Orbital velocity also increases as a function of wave period, which in the present example is 3 s. For a 10 cm wave—easily produced in most laboratory settings—u_b varies between 50 cm/s and 30 cm/s for water depths of 10 and 30 cm, respectively.

Table 1 presents a possible test matrix of combined flow processes in a laboratory setting. The wave heights needed to produce a range of bottom wave conditions are easily generated in most laboratory facilities.

Figure 8. Contour plot depicting u_b as a function of water depth and wave height. Values are derived from linear wave theory and are appropriate for laboratory-scale investigations.

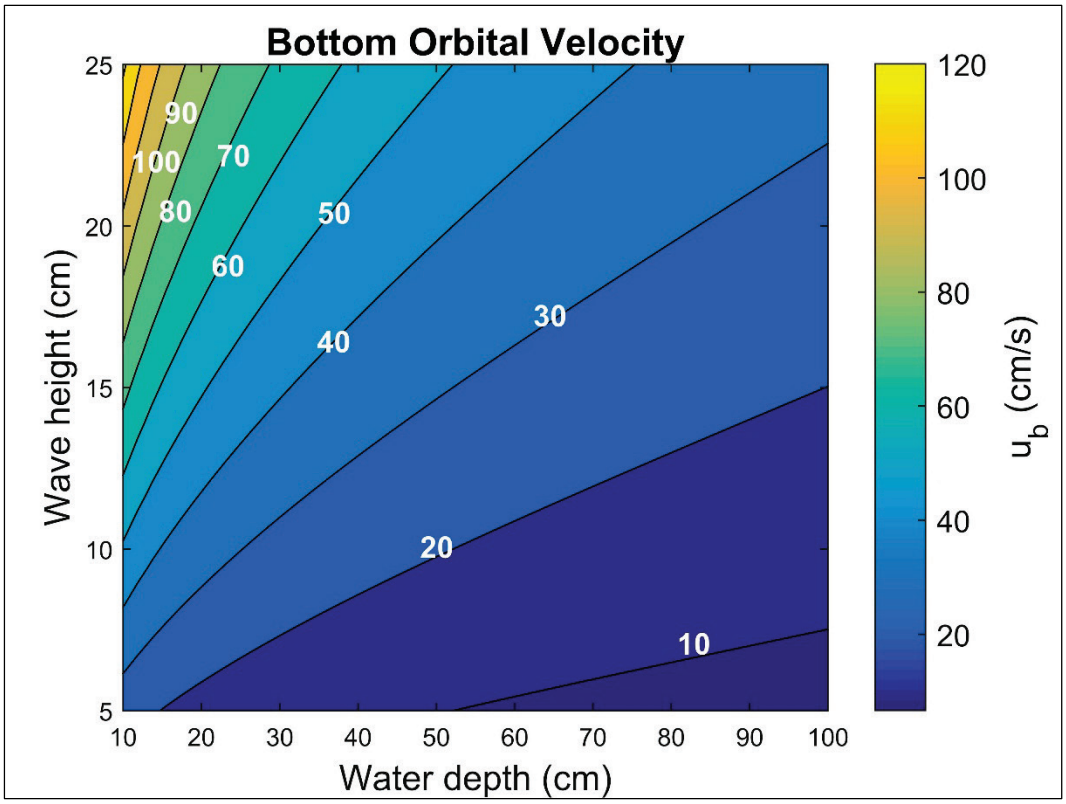

Table 1. Test matrix to examine wave and current boundary layer processes. The numbers denote the required wave height (cm) needed to produce the corresponding u_b.

Laboratory Wave Conditions							
	Offshore h= 50 cm			Breaker Edge h=15 cm			
	u_b= 0	u_b= 25	u_b= 50	u_b= 0	u_b= 25	u_b= 50	
u_r = 0	N/A	14	32	N/A	7	13	For T = 1.5 s wave
u_r = 25	N/A	14	32	N/A	7	13	
u_r = 50	N/A	14	32	N/A	7	13	
u_r = 0	N/A	13	24	N/A	6	12	For T = 3 s wave
u_r = 25	N/A	13	24	N/A	6	12	
u_r = 50	N/A	13	24	N/A	6	12	

References

Allen, J. S., R. C. Beardsley, W. S. Brown, D. A. Cacchione, R. E. Davis, D. E. Drake, C. Friehe, W. D. Grant, A. Huyer, J. D. Irish, M. M. Janopaul, A. J. Williams, and C. C. Winant. 1982. *A preliminary description of the CODE-1 field program*. Woods Hole: Woods Hole Oceanographic Institution.

Amoudry, L. O., and A. J. Souza. 2011. Deterministic coastal morphological and sediment transport modeling: A review and discussion. *Reviews of Geophysics* 49.

Bagnold, R. A. 1946. Motion of waves in shallow water interaction between waves and sand bottoms. In *Proceedings of the Royal Society of London, Series A 187*, 1–15.

Berni, C., E. Barthelemy, and H. Michallet. 2013. Surf zone cross-shore boundary layer velocity asymmetry and skewness: An experimental study on a mobile bed. *Journal of Geophysical Research-Oceans* 118:2188–2200.

Bever, A. J., C. K. Harris, C. R. Sherwood, and R. P. Signell. 2009. Deposition and flux of sediment from the Po River, Italy: An idealized and wintertime numerical modeling study. *Marine Geology* 260:69–80.

Businger, J. A., J. C. Wyngaard, Y. Izumi, and E. F. Bradley. 1971. Flux-profile relationships in the atmospheric surface layer. *Journal of the Atmospheric Sciences* 28:181–189.

Cacchione, D. A., W. D. Grant, D. E. Drake, and S. M. Glenn. 1987. Storm-dominated bottom boundary layer dynamics on the Northern California continental shelf: *Measurements and Predictions* 92 C2:1817–1827.

Carstens, M. R., F. M. Neilson, and H. D. Altinbilek. 1969. *Bed forms generated in the laboratory under an oscillatory flow: Analytical and experimental study*. U.S. Army Corps of Engineers: Coastal Engineering Research Center, 39.

Chen, J. L., F. Y. Shi, T. J. Hsu, and J. T. Kirby. 2014. NearCoM-TVD - A quasi-3D nearshore circulation and sediment transport model. *Coastal Engineering* 91:200–212.

Christoffersen, J. B., and I. G. Jonsson. 1985. Bed friction and dissipation in a combined current and wave motion. *Ocean Engineering* 12:387–423.

Chu, V. H., and C. C. Mei. 1970. On slowly-varying Stokes waves. *Journal of Fluid Mechanics* 41:873–887.

Dalrymple, R. A., and P. L. Liu. 1978. Waves over soft muds: A two-layer fluid model. *Journal of Physical Oceanography* 8:1121–1131.

Davies, A. G., R. L. Soulsby, and H. L. King. 1988. A numerical model of the combined wave and current bottom boundary layer. *Journal of Geophysical Research* 93:491–508.

De Wit, P., and C. Kranenburg. 1996. On the effects of a liquefied mud bed on wave and flow characteristics. *Journal of Hydraulic Research* 34:3–18.

Dean, R. G., and R. A. Dalrymple. 1991. *Water wave mechanics for engineers and scientists*. New Jersey: World Scientific.

Dingler, J. R., and D. L. Inman. 1976. Wave-formed ripples in nearshore sands. *Coastal Engineering Proceedings* 1.

Doucette, J., and T. O'Donoghue. 2006. Response of sand ripples to change in oscillatory flow. *Sedimentology* 53:581–596.

Drake, D. E., D. A. Cacchione, and W. D. Grant. 1992. Shear-stress and bed roughness estimates for combined wave and current flows over a rippled bed. *Journal of Geophysical Research-Oceans* 97:2319–2326.

Engelstad, A., T. Janssen, T. H. C. Herbers, G. van Vledder, S. Elgar, B. Raubenheimer, L. Trainor, and A. Garcia-Garcia. 2013. Wave evolution across the Louisiana shelf. *Continental Shelf Research* 52:190–202.

Faraci, C., E. Foti, and R. Musumeci. 2008. Waves plus currents at a right angle: The rippled bed case. *Journal of Geophysical Research: Oceans (1978–2012)* 113.

Foda, M. A., J. R. Hunt, and H. T. Chou. 1993. A nonlinear model for the fluidization of marine mud by waves. *Journal of Geophysical Research: Oceans (1978–2012)* 98:7039–7047.

Foster, D. L., R. A. Guenther, and R. A. Holman. 1999. An analytic solution to the wave bottom boundary layer governing equation under arbitrary wave forcing. *Ocean Engineering* 26:595–623.

Fox, J., P. Hill, T. Milligan, and A. Boldrin. 2004. Flocculation and sedimentation on the Po River Delta. *Marine Geology* 203:95–107.

Fredsøe, J. 1984. Turbulent boundary layer in wave-current motion. *Journal of Hydraulic Engineering* 110:1103–1120.

Glenn, S. M., and W. D. Grant. 1987. A suspended sediment stratification correction for combined wave and current flows. *Journal of Geophysical Research-Oceans* 92:8244–8264.

Grant, W. D. 1977. *Bottom friction under waves in the presence of a weak current: Its relationship to coastal sediment transport*. Cambridge: Massachusetts Institute of Technology, 275.

Grant, W. D., and O. S. Madsen. 1979. Combined wave and current interaction with a rough bottom. *Journal of Geophysical Research* 84:1797–1808.

Grant, W. D., and O. S. Madsen. 1982. Movable bed roughness in unsteady oscillatory flow. *Journal of Geophysical Research* 87:469–481.

Grant, W. D., and O. S. Madsen. 1986. The continental-shelf bottom boundary layer. *Annual Review of Fluid Mechanics* 18:265–305.

Grant, W. D., A. J. Williams, III, and S. M. Glenn. 1984. Bottom stress estimates and their prediction on the northern California continental shelf during CODE-1: The importance of wave-current interaction. *Journal of Physical Oceanography* 14:506–527.

Gross, T. F., A. E. Isley, and C. R. Sherwood. 1992. Estimation of stress and bed roughness during storms on the Northern California shelf. *Continental Shelf Research* 12 :389–413.

Guza, R., E. Thornton, and N. Christensen, Jr. 1986. Observations of steady longshore currents in the surf zone. *Journal of Physical Oceanography* 16:1959–1969.

Inman, D. L. 1957. *Wave-generated ripples in nearshore sands*. Washington, DC: U.S. Beach Erosion Board, 40.

Jain, M., and A. J. Mehta. 2009. Role of basic rheological models in determination of wave attenuation over muddy seabeds. *Continental Shelf Research* 29:642–651.

Jensen, B., B. Sumer, and J. Fredsøe. 1989. Turbulent oscillatory boundary layers at high Reynolds numbers. *Journal of Fluid Mechanics* 206:265–297.

Jonsson, I. G., and N. A. Carlsen. 1976. Experimental and theoretical investigations in an oscillatory turbulent boundary layer. *Journal of Hydraulic Research* 14:45–60.

Kobayashi, N., A. Payo, and L. Schmied. 2008. Cross-shore suspended sand and bed load transport on beaches. *Journal of Geophysical Research: Oceans (1978–2012)* 113.

Komar, P. D. 1975. Nearshore currents: Generated by oblique incident waves and longshore variations in breaker heights.In *Nearshore Sediment Dynamics and Sedimentation*, ed. J. Hails and A. Carr, 18–45. London: Wiley.

Komar, P. D. 1998. *Beach processes and sedimentation, 2nd ed.* Upper Saddle River: Prentice Hall.

Kranenburg, W. M., J. S. Ribberink, R. E. Uittenbogaard, and S. Hulscher. 2012. Net currents in the wave bottom boundary layer: On waveshape streaming and progressive wave streaming. *Journal of Geophysical Research-Earth Surface* 117:18.

Kraus, N., and T. Sasaki. 1979. Influence of wave angle and lateral mixing on the longshore current. *Marine Science Communications* 5:91–126.

Lamb, M. P., E. D'Asaro, and J. D. Parsons. 2004. Turbulent structure of high-density suspensions formed under waves. *Journal of Geophysical Research-Oceans* 109.

Larson, M., and N. C. Kraus. 1991. Numerical model of longshore current for bar and trough beaches. *Journal of Waterway, Port, Coastal, and Ocean Engineering* 117:326–347.

Lee, T. H., and D. M. Hanes. 1996. Comparison of field observations of the vertical distribution of suspended sand and its prediction by models. *Journal of Geophysical Research-Oceans* 101:3561–3572.

Li, M., and B. A. O'Connor. 2007. Numerical study of sediment transport above rippled beds under the action of combined waves and currents. *Sedimentology* 54:1345–1363.

Li, M. Z., and C. L. Amos. 1998. Predicting ripple geometry and bed roughness under combined waves and currents in a continental shelf environment. *Continental Shelf Research* 18:941–970.

Longuet-Higgins, M. S. 1953. Mass transport in water waves. *Phil. Trans. Roy. Soc. Series A* 245:535–581.

Longuet-Higgins, M. S. 1970. Longshore currents generated by obliquely incident sea waves: 1. *Journal of Geophysical Research* 75:6778–6789.

Lumley, J. 1978. *Two-phase and non-Newtonian flows, turbulence*. Berlin: Springer, 289–324.

Lundgren, H. 1972. Turbulent currents in the presence of waves. In *13th International Conference on Coastal Engineering, Vancouver*, 623–634.

Lynch, J. F., J. D. Irish, T. F. Gross, P. L. Wiberg, A. E. Newhall, P. A. Traykovski, and J. D. Warren. 1997. Acoustic measurements of the spatial and temporal structure of the near-bottom boundary layer in the 1990-1991 STRESS experiment. *Continental Shelf Research* 17:1271–1295.

Lynch, J. F., J. D. Irish, C. R. Sherwood, and Y. C. Agrawal. 1994. Determining suspended sediment particle-size information from acoustical and optical backscatter measurements. *Continental Shelf Research* 14:1139–1165.

Maa, J. P.-Y., and A. J. Mehta. 1988. Soft mud properties: Voigt model. *Journal of Waterway, Port, Coastal, and Ocean Engineering* 114:765–770.

Madsen, O. S., D. W. Ostendorf, and A. S. Reyman. 1978. *A longshore current model, coastal zone '78*. Reston, VA: ASCE, 2332–2341.

Madsen, O. S., and P. N. Wikramanayake. 1991. *Simple models for turbulent wave-current bottom boundary layer flow*. Vicksburg, MS: U.S. Army Corps of Engineers, 150.

Madsen, O. S., L. D. Wright, J. D. Boon, and T. A. Chisholm. 1993. Wind stress, bed roughness and sediment suspension on the inner shelf during an extreme storm event. *Continental Shelf Research* 13:1303–1324.

Malarkey, J., and A. Davies. 1998. Modelling wave–current interactions in rough turbulent bottom boundary layers. *Ocean Engineering* 25:119–141.

Mallard, W. W., and R. A. Dalrymple. 1977. Water waves propagating over a deformable bottom. In *Proceedings, Ninth Annual Offshore Technology Conference, Houston, TX*.

Mathisen, P. P., and O. S. Madsen. 1996. Waves and currents over a fixed rippled bed .1. Bottom roughness experienced by waves in the presence and absence of currents. *Journal of Geophysical Research-Oceans* 101:16533–16542.

McClennen, C. E. 1973. Sands on continental shelf off New Jersey move in response to waves and currents. *Maritimes* 17:14–16.

Mehta, A. J., E. J. Hayter, W. R. Parker, R. B. Krone, and A. M. Teeter. 1989. Cohesive sediment transport .1. Process description. *Journal of Hydraulic Engineering-ASCE* 115:1076–1093.

Mei, C. C., M. Krotov, Z. H. Huang, and A. Huhe. 2010. Short and long waves over a muddy seabed. *Journal of Fluid Mechanics* 643:33–58.

Ng, C. O. 2000. Water waves over a muddy bed: A two-layer Stokes' boundary layer model. *Coastal Engineering* 40:221–242.

Ng, C. O., and X. Y. Zhang. 2007. Mass transport in water waves over a thin layer of soft viscoelastic mud. *Journal of Fluid Mechanics* 573:105–130.

Nielsen, P. 1981. Dynamics and geometry of wave-generated ripples. *Journal of Geophysical Research* 86:6467–6472.

Nielsen, P. 1984. Field measurements of time-averaged suspended sediment concentrations under waves. *Coastal Engineering* 8:51–72.

Nielsen, P. 1992. *Coastal bottom boundary layers and sediment transport*. New York: World Scientific.

Papanicolaou, A. N., M. Elhakeem, G. Krallis, S. Prakash, and J. Edinger. 2008. Sediment transport modeling review—current and future developments. *Journal of Hydraulic Engineering* 134:1–14.

Rouse, H. 1937. Modern conceptions of the mechanics or fluid turbulence. *Transactions of the American Society of Civil Engineers* 102:463–505.

Safak, I., C. Sahin, J. M. Kaihatu, and A. Sheremet. 2013. Modeling wave-mud interaction on the central chenier-plain coast, western Louisiana Shelf, USA. *Ocean Modelling* 70:75–84.

Sahin, C., I. Safak, A. Sheremet, and A. J. Mehta. 2012. Observations on cohesive bed reworking by waves: Atchafalaya Shelf, Louisiana. *Journal of Geophysical Research-Oceans* 117:14.

Sakakiyama, T., and E. W. Byker. 1989. Mass transport velocity in mud layer due to progressive waves. *Journal of Waterway, Port, Coastal, and Ocean Engineering* 115:614–633.

Schofield, O., T. Bergmann, P. Bissett, J. F. Grassle, D. B. Haidvogel, J. Kohut, M. Moline, and S. M. Glenn. 2002. The long-term ecosystem observatory: An integrated coastal observatory. *IEEE Journal of Oceanic Engineering* 27:146–154.

Sherwood, C. R., B. Butman, D. A. Cacchione, D. E. Drake, T. F. Gross, R. W. Sternberg, P. L. Wiberg, and A. J. Williams. 1994. Sediment-transport events on the Northern California continental-shelf during the 1990–1991 stress experiment. *Continental Shelf Research* 14:1063–1099.

Shi, J. Z., and Y. Wang. 2008. The vertical structure of combined wave–current flow. *Ocean Engineering* 35:174–181.

Sleath, J. F. A. 1987. Turbulent oscillatory flow over rough beds. *Journal of Fluid Mechanics* 182:369–409.

Smith, D., and J. F. Sleath. 2005. Transient ripples in oscillatory flows. *Continental Shelf Research* 25:485–501.

Smith, J. D. 1977. Modeling of sediment transport on continental shelves. In *The Sea*, ed. D. Goldberg, I. N. McCave, J. J. O'Brien, and J. H. Steele, Interscience, 538–577.

Soltanpour, M., S. A. Haghshenas, and A. J. Mehta. 2009. Fluidized mud-wave interaction under regular and irregular waves. *Journal of Coastal Research* 25:616–626.

Sorenson, K., O. Madsen, and L. Wright. 1995. Evidence of directional-dependence of moveable bottom roughness in inner shelf waters. *Eos Trans. AGU* 76:46.

Soulsby, R. 1997. *Dynamics of marine sands: A manual for practical applications*. Thomas Telford.

Soulsby, R., L. Hamm, G. Klopman, D. Myrhaug, R. Simons, and G. Thomas. 1993. Wave-current interaction within and outside the bottom boundary layer. *Coastal Engineering* 21:41–69.

Stull, R. B. 1988. *An introduction to boundary layer meteorology*. Berlin: Springer Science and Business Media.

Styles, R., and S. M. Glenn. 2000. Modeling stratified wave and current bottom boundary layers on the continental shelf. *Journal of Geophysical Research-Oceans* 105:24119–24139.

Styles, R., and S. M. Glenn. 2002. Modeling bottom roughness in the presence of wave-generated ripples. *Journal of Geophysical Research-Oceans* 107:24/21, 24/15.

Testik, F., S. Voropayev, and H. Fernando. 2005. Adjustment of sand ripples under changing water waves. *Physics of Fluids (1994–present)* 17:072104.

Thornton, E. B., and R. T. Guza. 1986. Surf zone longshore currents and random waves: Field data and models. *Journal of Physical Oceanography* 16:1165–1178.

Tolman, H. L. 1994. Wind-waves and moveable-bed bottom friction. *Journal of Physical Oceanography* 24:994–1009.

Traykovski, P. 2007. Observations of wave orbital scale ripples and a nonequilibrium time-dependent model. *Journal of Geophysical Research: Oceans (1978–2012)* 112.

Traykovski, P., A. E. Hay, J. D. Irish, and J. F. Lynch. 1999. Geometry, migration, and evolution of wave orbital ripples at LEO-15. *Journal of Geophysical Research-Oceans* 104:1505–1524.

Trowbridge, J., and O. S. Madsen. 1984. Turbulent wave boundary layers 2. Second-order theory and mass transport. *Journal of Geophysical Research* 89:7999–8007.

Trowbridge, J. H., and Y. C. Agrawal. 1995. Glimpses of a wave boundary-layer. *Journal of Geophysical Research-Oceans* 100:20729–20743.

Van Doorn, T. 1981. *Experimental investigation of near bottom velocities in water waves with and without a current*. Report M1423. Delft, The Netherlands: Delft Hydraulics Laboratory.

Van Rijn, L., P. Tonnon, and D. Walstra. 2011. Numerical modelling of erosion and accretion of plane sloping beaches at different scales. *Coastal Engineering* 58:637–655.

Van Rijn, L. C. 2007a. Unified view of sediment transport by currents and waves. I: Initiation of motion, bed roughness, and bed-load transport. *Journal of Hydraulic Engineering* 133:649–667.

Van Rijn, L. C. 2007b. Unified view of sediment transport by currents and waves. II: Suspended transport. *Journal of Hydraulic Engineering* 133:668–689.

Villaret, C., and J. H. Trowbridge. 1991. Effects of stratification by suspended sediments on turbulent shear flows. *Journal of Geophysical Research-Oceans* 96:10659–10680.

von Alt, C. J., and J. Grassle. 1992. LEO-15–an unmanned long-term environmental observatory. *Proc. Oceans*, 849–854.

Wiberg, P., and J. D. Smith. 1983. A comparison of field data and theoretical models for wave-current interactions at the bed on the continental shelf. *Continental Shelf Research* 2:147–162.

Wiberg, P. L., D. E. Drake, and D. A. Cacchione. 1994. Sediment resuspension and bed armoring during high bottom stress events on the Northern California Inner Continental-Shelf - measurements and predictions. *Continental Shelf Research* 14:1191–1219.

Wiberg, P. L., and C. K. Harris. 1994. Ripple geometry in wave-dominated environments. *Journal of Geophysical Research-Oceans* 99:775–789.

Wikramanayake, P. N., and O. S. Madsen. 1991. *Calculation of movable bed friction factors*. Technical Progress Report, 1–105.

Wikramanayake, P. N., and O. S. Madsen. 1992. *Calculation of suspended sediment transport by combined wave-current flows*. Vicksburg, MS: U.S. Army Corps of Engineers, 148.

Wilson, G. W., A. E. Hay, and A. J. Bowen. 2014. Observations of wave shear stress on a steep beach. *Journal of Geophysical Research-Oceans* 119:7827–7839.

Wilson, K. 1989. Friction of wave-induced sheet flow. *Coastal Engineering* 12:371–379.

Winterwerp, J. C., and W. G. Van Kesteren. 2004. *Introduction to the physics of cohesive sediment dynamics in the marine environment*. Philadelphia, PA: Elsevier.

Wooding, R. A., E. F. Bradley, and J. K. Marshall. 1973. Drag due to regular arrays of roughness elements of varying geometry. *Boundary-Layer Meteorology* 5:285–308.

Wright, L. D., J. D. Boon, S. C. Kim, and J. H. List. 1991. Modes of cross-shore sediment transport on the shoreface of the Middle Atlantic Bight. *Marine Geology* 96:19–51.

You, Z.-J. 1996. Movable bed roughness and current profiles in the presence of irregular waves with an arbitrary angle to currents. *Ocean Engineering* 23:225–242.

Zhao, Z. D., J. J. Lian, and J. Z. Shi. 2006. Interactions among waves, current, and mud: Numerical and laboratory studies. *Advances in Water Resources* 29:1731–1744.

Zou, Q., and A. E. Hay. 2003. The vertical structure of the wave bottom boundary layer over a sloping bed: Theory and field measurements. *Journal of Physical Oceanography* 33:1380–1400.

Zou, Q., A. E. Hay, and A. J. Bowen. 2003. Vertical structure of surface gravity waves propagating over a sloping seabed: Theory and field measurements. *Journal of Geophysical Research: Oceans (1978–2012)* 108.

REPORT DOCUMENTATION PAGE

Form Approved
OMB No. 0704-0188

1. REPORT DATE	2. REPORT TYPE	3. DATES COVERED *(From - To)*
March 2016	**Special Report**	

4. TITLE AND SUBTITLE

Combined Wave and Current Bottom Boundary Layers: A Review

5a. CONTRACT NUMBER

5b. GRANT NUMBER

5c. PROGRAM ELEMENT NUMBER

6. AUTHOR(S)

Richard Styles and Duncan Bryant

5d. PROJECT NUMBER

5e. TASK NUMBER

5f. WORK UNIT NUMBER

7. PERFORMING ORGANIZATION NAME(S) AND ADDRESS(ES)
U.S. Army Corps of Engineers
Engineer Research and Development Center
Coastal and Hydraulics Laboratory
3909 Halls Ferry Road, Vicksburg, MS 39180

8. PERFORMING ORGANIZATION REPORT NUMBER

ERDC/CHL SR-16-1

9. SPONSORING/MONITORING AGENCY NAME(S) AND ADDRESS(ES)

10. SPONSOR/MONITOR'S ACRONYM(S)

11. SPONSOR/MONITOR'S REPORT NUMBER(S)

12. DISTRIBUTION/AVAILABILITY STATEMENT

Approved for public release; distribution is unlimited.

13. SUPPLEMENTARY NOTES

14. ABSTRACT

This Coastal and Hydraulics Engineering Special Report (SR) presents a general review of research in combined wave and current bottom boundary layers including laboratory, field and model studies. The purpose of this SR is to chronicle the state-of-the-art in boundary layer research in order to identify research gaps and obtain guidance for developing and improving the next generation of combined wave and current bottom boundary layer models. One of the key research focus areas identified in this report is fine-grained sediment transport processes in combined wave and current flows. Critical research gaps exist in the following areas: (1) the role of oblique waves and currents on bottom stress and flow kinematics, (2) the effect of wave asymmetry in combined flows and how this drives mass transport, (3) the process of wave transition in shallow water in the presence of strong alongshore currents, (4) the interaction between oblique waves and currents over a sediment bottom, and (5) the validity and performance limitations of existing bottom boundary layer models under the above conditions. Progress towards understanding these research questions hinges on experimental programs to measure sediment, waves, morphology, and currents under a range of forcing conditions.

15. SUBJECT TERMS

Bed roughness, Bottom stress, Boundary layers, Models, Near-shore processes, Review article, Sediment transport, Wave and current interaction

16. SECURITY CLASSIFICATION OF:			17. LIMITATION OF ABSTRACT	18. NUMBER OF PAGES	19a. NAME OF RESPONSIBLE PERSON
a. REPORT	b. ABSTRACT	c. THIS PAGE			Richard Styles
Unclassified	Unclassified	Unclassified	SAR	56	19b. TELEPHONE NUMBER *(Include area code)* 601-634-4065